Curcumenol inhibits malignant progression and promotes ferroptosis via the SLC7A11/NF-κB/TGF-β pathway in triple-negative breast cancer

FEIFEI LI[1-4*], QIN QI[1,2*], YU QIAO[1,2], YAN HUANG[1,2], YUAN LU[1,2], KAN GU[1,2], HUIRONG LIU[1,2], CHUNFANG GAO[1], SHENG LIU[3,4] and HUANGAN WU[1,2]

[1]Medical Laboratory, Yueyang Hospital of Integrated Traditional Chinese and Western Medicine, Shanghai University of Traditional Chinese Medicine, Shanghai 200437, P.R. China; [2]Immunology Laboratory, Shanghai Research Institute of Acupuncture and Meridian, Shanghai 200030, P.R. China; [3]Hospital Management Office, Shanghai University of Traditional Chinese Medicine, Shanghai 201203, P.R. China; [4]Integrated Traditional Chinese and Western Medicine Breast Department, Longhua Hospital, Shanghai University of Traditional Chinese Medicine, Shanghai 200030, P.R. China

Received December 6, 2024; Accepted Aprill 8, 2025

DOI: 10.3892/ijmm.2025.5552

Abstract. Triple-negative breast cancer (TNBC) exhibits a high degree of malignancy and a propensity for metastasis, ultimately resulting in unfavorable patient outcomes. *Curcuma phaeocaulis* Valeton is a common herb used in traditional Chinese medicine to treat TNBC. Curcumenol (Cur) is a natural compound derived from *C. phaeocaulis* Valeton, the effects of which on breast cancer remain under-reported. The present study elucidated that Cur could effectively inhibit the survival ability of TNBC cells and enhance their sensitivity to paclitaxel. Western blotting (WB) further revealed that Cur modulated apoptosis and epithelial-mesenchymal transition (EMT) in TNBC. Findings from animal experiments further validated these observations. In the established TNBC mouse model, Cur was shown to exert an inhibitory effect on tumor growth, effectively attenuate EMT and substantially reduce the incidence of lung metastasis. Integrated analyses using RNA sequencing, WB and reverse transcription-quantitative polymerase chain reaction demonstrated that Cur markedly downregulated the expression levels of solute carrier family 7 member 11 (SLC7A11), phosphorylated-NF-κB and TGF-β. Molecular docking studies further validated that Cur can establish stable interactions with SLC7A11. In-depth bioinformatics analysis revealed a positive association between high SLC7A11 expression and reduced disease-free survival in patients with breast cancer. Additionally, in TNBC cells, Cur was revealed to reduce the mitochondrial membrane potential and promote the accumulation of lipid reactive oxygen species. Subsequent experimental investigations demonstrated that Cur can counteract the inhibitory influence of ferrostatin-1 on ferroptosis. These findings strongly implied a potential underlying mechanism, suggesting that Cur may impede the malignant progression of TNBC via the modulation of ferroptosis. In conclusion, the findings of the present study underscore the marked efficacy of Cur in hampering the progression of TNBC by suppressing the SLC7A11/NF-κB/TGF-β signaling pathway.

Correspondence to: Professor Huangan Wu, Medical Laboratory, Yueyang Hospital of Integrated Traditional Chinese and Western Medicine, Shanghai University of Traditional Chinese Medicine, 110 Ganhe Road, Hongkou, Shanghai 200437, P.R. China
E-mail: wuhuangan@126.com

Professor Sheng Liu, Integrated Traditional Chinese and Western Medicine Breast Department, Longhua Hospital, Shanghai University of Traditional Chinese Medicine, 725 Wanping South Road, Xuhui, Shanghai 200030, P.R. China
E-mail: lhliusheng@163.com

*Contributed equally

Key words: curcumenol, triple-negative breast cancer, lung metastasis, epithelial-mesenchymal transition, ferroptosis

Introduction

Breast cancer is a leading cause of death among women, with its incidence showing an upward trend (1). According to the 2024 cancer statistics, 310,700 new cases of breast cancer and 42,200 breast cancer-related deaths were recorded among women globally, ranking second in incidence among cancers in women (2). Compared with other subtypes of breast cancer, triple-negative breast cancer (TNBC) exhibits a higher incidence in premenopausal women and is characterized by significant molecular heterogeneity. TNBC is characterized by poor differentiation, high invasiveness, and a propensity for recurrence and metastasis (3). Notably, more than one-third of patients with TNBC experience recurrence or distant metastasis (4). The IMpassion132 study showed that the median progression-free survival time for patients with TNBC with early recurrent, unresectable, locally advanced or metastatic cancer is 4 months, indicating a poor prognosis (5). The efficacy of combined chemotherapy regimens and immunotherapy for TNBC is being actively explored (6,7). In addition, traditional

Chinese medicine (TCM) has shown efficacy in the treatment of TNBC, demonstrating potential in enhancing chemotherapy sensitivity (8) and prolonging disease-free survival (DFS), and has thus gradually gained international recognition. In our previous study, it was demonstrated that incorporating Sanyin Formula into standard chemotherapy can improve the 5-year DFS rate of patients with TNBC, increasing it from 85.5 to 94.2%. Notably, this herbal formulation has since been approved as a hospital-prepared medicinal product and is currently undergoing expanded clinical implementation (9).

TCM employs a wide range of natural products as therapeutic agents for the treatment of various diseases and conditions (10). *Curcuma phaeocaulis* Valeton is commonly used as a TCM for breast cancer treatment (11). Various chemical components of *C. phaeocaulis* Valeton, including curcumenol (Cur), β-elemene and curcumin, have been reported to exhibit anti-breast cancer capabilities (12).

Cur, a main active component of *C. phaeocaulis* Valeton, has been demonstrated to exert antitumor effects on lung cancer by triggering ferroptosis (13). In cervical cancer, Cur can reduce cell proliferation and invasion when combined with cisplatin (14). However, to the best of our knowledge, the inhibitory effects of Cur on TNBC have not yet been thoroughly reported. Therefore, the current study aimed to investigate the therapeutic effects and potential mechanisms of Cur in TNBC, with the goal of providing a safe and effective natural product for TNBC treatment. A flowchart summarizing the research methods performed in the present study is shown in Fig. 1.

Materials and methods

Chemicals. Cur (purity ≥98%; Shanghai Yuanye Biotechnology Co., Ltd.) and paclitaxel (PTX; Abmole Bioscience Inc.) were dissolved in dimethyl sulfoxide (Shanghai Yeasen Biotechnology Co., Ltd.). Ferrostatin-1 (Fer-1; MedChemExpress) was dissolved in sterile water (Shanghai Yeasen Biotechnology Co., Ltd.).

Cell culture. The TNBC cell lines 4T1 and MDA-MB-231 were cultured in Roswell Park Memorial Institute (RPMI) 1640 and Dulbecco's modified Eagle's medium (DMEM), respectively (both from The Cell Bank of Type Culture Collection of The Chinese Academy of Sciences). All culture media were supplemented with 10% fetal bovine serum (FBS; Gibco; Thermo Fisher Scientific, Inc.) and 1% penicillin/streptomycin (Gibco; Thermo Fisher Scientific, Inc.). The cells were incubated at 37˚C within a humidified incubator containing 5% CO_2 to guarantee optimal growth conditions.

Animal experiment. A total of 20 specific pathogen-free female BALB/c mice (age, 6 weeks; weight, ~20 g) were obtained from Shanghai Lingchang Biotechnology Co., Ltd., and were divided into four groups (n=5 mice/group). The mice were housed in a controlled environment, where the temperature was maintained at 22±2˚C and the relative humidity was set at 50±10%. The mice had *ad libitum* access to standard rodent chow and fresh water, and were maintained under a 12-h light/dark cycle. Animals were subcutaneously injected with $5x10^4$ 4T1 cells after 1 week of adaptive feeding. When tumors reached a volume of 100 mm^3, the mice were allocated at random into the following four groups: Mice in the model group received 100 μl saline every 2 days; mice in the positive group were administered PTX at a dose of 10 mg/kg every 7 days; mice in the Cur treatment groups were administered 5 or 10 mg/kg Cur every 2 days. All treatments were administered intraperitoneally and lasted for 3 weeks. Mice were euthanized by gradual-fill CO_2 inhalation at a displacement rate of 30% chamber volume/min, sustained for ≥5 min. Death was confirmed through the absence of breathing, loss of muscle tone and mice were cervically dislocated after being subjected to CO_2 inhalation. The following criteria were established as humane endpoints: i) Weight loss exceeding 20% of the initial body weight; ii) Tumor growth reaching more than 10% of the body weight, the average tumor diameter in mice surpassing 20 mm, or rapid tumor growth leading to ulceration, which in turn caused infection or necrosis; iii) inability of the mice to eat, drink or maintain an upright stance; iv) in non-anesthetized or non-sedated animals, signs of depression (such as immobility, excessive sniffing, trembling and scratching) accompanied by a body temperature <37˚C, abnormal central nervous system responses (excessive excitement or inhibitory behavioral responses) and an inability to effectively manage pain (when being touched or slight pressure was applied, the mice showed abnormal struggling and squeaking). No mice reached any of the humane endpoints during the study. The present study was approved by the Animal Welfare Committee of Longhua Hospital, Shanghai University of TCM (approval no. LHERAW-24010; Shanghai, China).

Cell counting kit-8 (CCK-8) assay. The TNBC cell lines 4T1 and MDA-MB-231 were seeded into 96-well plates at a density of 5,000 cells/well, and were then exposed to multiple doses of Cur (0, 6.25, 12.5, 25, 50, 100, 200 and 400 μM) and PTX (50 and 500 nM) at 37˚C for 24 and 48 h. Following treatment, the cells were incubated with the CCK-8 reagent (Beyotime Institute of Biotechnology) for 2 h at 37˚C and cell viability was determined. The IC_{50} values were calculated by nonlinear regression analysis of dose-response curves (GraphPad Prism Version 10.1; Dotmatics) using a four-parameter logistic model.

Wound healing assay. A 1-ml pipette tip was used to make a scratch across 4T1 and MDA-MB-231 cells that had reached 80-90% confluence in 6-well plates. Subsequently, the cells were exposed to 25, 50 and 100 μM Cur at 37˚C for 24 and 48 h in serum-free media. Images were captured using an IX71 inverted light microscope (Olympus Corporation).

Invasion assay. After 24 h of exposure to 25, 50 and 100 μM Cur at 37˚C, the 4T1 and MDA-MB-231 cells were seeded into 24-well Transwell inserts (8-μm pore size), which were precoated with Matrigel at 37˚C for 2 h. A total of $5x10^4$ cells/well serum-free medium were plated in the upper chamber. Cells were then permitted to migrate into the lower chamber, which contained medium supplemented with 20% FBS at 37˚C for 24 h. Then, the migrated cells were fixed with 4% paraformaldehyde at room temperature for 15 min and stained with 0.1% crystal violet at room temperature for 15 min. The number of invasive cells was counted from each sample using a light microscope.

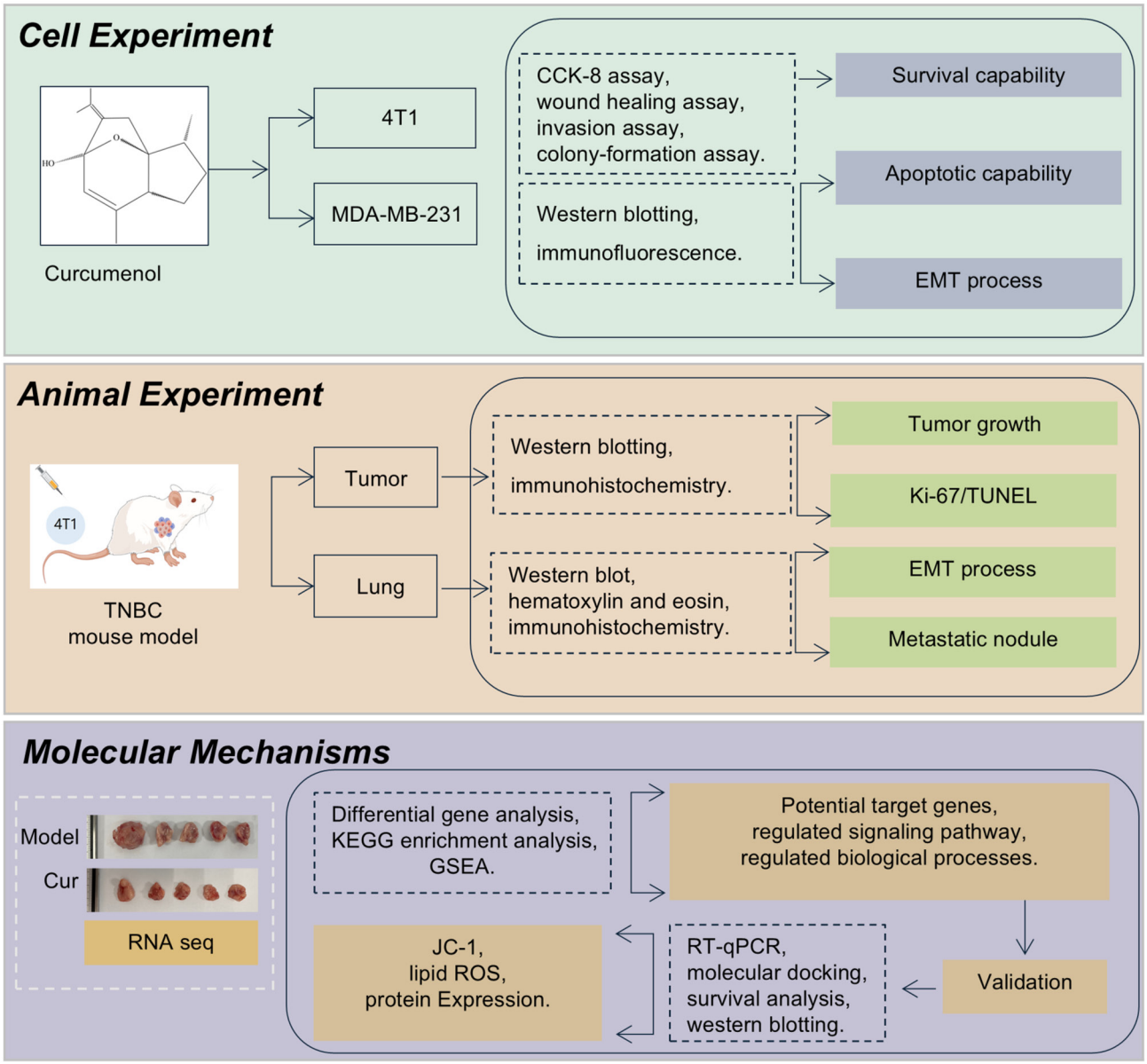

Figure 1. Research flowchart. CCK-8, Cell Counting Kit-8; EMT, epithelial-mesenchymal transition; RNA seq, RNA sequencing; ROS, reactive oxygen species; RT-qPCR, reverse transcription-quantitative polymerase chain reaction.

Colony formation assay. 4T1 and MDA-MB-231 cells were first exposed to 25, 50 and 100 μM Cur at 37˚C for 24 h hand were then spread individually into 6-well plates at a density of 1,000 cells/well. The medium was changed every 2 days until colonies of cells gradually formed after 7-10 days. For colony fixation and staining, the colonies were fixed with 4% paraformaldehyde at room temperature for 15 min and then stained with 0.1% crystal violet at room temperature for 15 min. Colonies were defined as clusters of >50 cells and the colonies were quantified using ImageJ software (version 1.8.0, National Institutes of Health).

Western blotting (WB). Proteins were extracted from 4T1 and MDA-MB-231 cells and tumor tissues using radioimmunoprecipitation assay supplemented with phenylmethylsulfonyl fluoride and a phosphatase inhibitor (100:1:2; all purchased from Beyotime Institute of Biotechnology). The protein concentration in the lysate supernatants was determined using the bicinchoninic acid method. Subsequently, 30 μg proteins were loaded per lane and were separated by SDS-PAGE on 10% polyacrylamide gels. The proteins were then transferred onto PVDF membranes, which were blocked with a protein-free rapid blocking solution (Epizyme; Ipsen Pharma) at room temperature for 30 min. The membranes were then incubated with primary antibodies (1:1,000) at 4˚C for >12 h. The primary antibodies used were BCL-2 (cat. no. A19693; ABclonal Biotech Co., Ltd.), BAX (cat. no. A19684; ABclonal Biotech Co., Ltd.), caspase 3 (cat. no. 9662; Cell Signaling Technology, Inc.), cleaved caspase 3 (cat. no. 9664; Cell Signaling Technology, Inc.), caspase 9 (cat. no. 9508; Cell Signaling Technology, Inc.), cleaved caspase 9 (cat. no. 9509; Cell Signaling Technology, Inc.), cleaved caspase 9 (cat. no. 9505; Cell Signaling Technology, Inc.), E-cadherin (cat. no. 20874-1-AP; Proteintech Group, Inc.), N-cadherin (cat. no. 22018-1-AP; Proteintech Group, Inc.), Vimentin (cat. no. 5741; Cell Signaling Technology,

Inc.), acyl-CoA synthetase long-chain family member 4 (ACSL4; cat. no. A20414; ABclonal Biotech Co., Ltd.), SLC7A11 (cat. no. 26864-1-AP; Proteintech Group, Inc.), glutathione (GSH) peroxidase 4 (GPX4; cat. no. A11243; ABclonal Biotech Co., Ltd.), TGF-β (cat. no. A25313; ABclonal Biotech Co., Ltd.), NF-κB (cat. no. 10745-1-AP; Proteintech Group, Inc.) and phosphorylated (p-)NF-κB (cat. no. 82335-1-RR; Proteintech Group, Inc.). The loading controls used were β-actin (cat. no. AC026; ABclonal Biotech Co., Ltd.) and GAPDH (cat. no. A19056; ABclonal Biotech Co., Ltd.). After three washes with TBS-0.1% Tween (10 min each), the membranes were incubated with the corresponding secondary antibodies (1:5,000) for 1 h at room temperature. The secondary antibodies were HRP-conjugated goat anti-rabbit IgG (H+L) (cat. no. AS014; ABclonal Biotech Co., Ltd.) and HRP conjugated rabbit anti-mouse (cat. no. AS115; ABclonal Biotech Co., Ltd.) antibodies. The protein bands were visualized using an enhanced chemiluminescent kit (ABclonal Biotech Co., Ltd.) and the gray scale analysis of the bands was performed using ImageJ software to compare the relative expression levels of the target proteins in different samples.

JC-1 assay. After treatment with 100 μM Cur at 37˚C for 24 h, the JC-1 staining working solution (Beyotime Institute of Biotechnology) was added to the 6-well plate seeded with 4T1 and MDA-MB-231 cells ($1x10^6$/well). Subsequently, the cells underwent two washes with JC-1 staining buffer (Beyotime Institute of Biotechnology) and were subsequently supplemented with DMEM. Fluorescence was then observed using a confocal laser scanning microscope (Zeiss AG).

Immunofluorescence staining. After treatment with 100 μM Cur at 37˚C for 24 h, 4T1 and MDA-MB-231 cells were fixed in 4% paraformaldehyde at room temperature for 15 min and then permeabilized with 0.1% Triton X-100 (Beyotime Institute of Biotechnology) at room temperature for 5 min. After blocking with a protein-free rapid blocking solution at room temperature for 1 h, the cells were incubated with corresponding primary antibodies (1:200) and secondary antibodies (1:500). The cells were incubated with the corresponding primary antibodies at 4˚C overnight. The primary antibodies used were E-cadherin (cat. no. 14472; Cell Signaling Technology, Inc,) and Vimentin (cat. no. 5741; Cell Signaling Technology, Inc.). After washing, the cells were incubated with the following secondary antibodies (1:200) at room temperature for 1-2 h: FITC-conjugated goat anti-mouse IgG (H+L) (cat. no. AS001; ABclonal Biotech Co., Ltd.) and ABflo 555-conjugated goat anti-rabbit IgG (H+L) (cat. no. AS058; ABclonal Biotech Co., Ltd.). For nuclear staining, the cells were incubated with DAPI at a concentration 1 μg/ml at room temperature for 5 min. The images were captured using a confocal laser scanning microscope (Zeiss, Germany).

Assessment of lung metastatic nodes. Following fixation with Bouin's fixative solution (Fuzhou Phygene Biotechnology Co., Ltd.) at room temperature for 24 h, surface lung metastases from mice were counted and presented as the mean number of visible nodules per lung ± SD.

Hematoxylin and eosin (H&E) staining and immunohistochemistry (IHC). Preserved tumor tissues were fixed in 10% neutral-buffered formalin at room temperature for 24 h, embedded in paraffin and sliced into 5 μm sections. The paraffin-embedded sections were then deparaffinized twice in xylene at 60˚C (10 min each). Subsequently, they were rehydrated in a descending alcohol series [100% ethanol twice (5 min each), 95% ethanol for 5 min, 80% ethanol for 5 min and 70% ethanol for 5 min], followed by a wash in distilled water. Antigen retrieval was performed by heating the sections in citrate buffer (pH 6.0) at 95-100˚C for 20 min, after which, the sections were allowed to cool at room temperature for 30 min. For intracellular antigens or membrane proteins with an internal epitope, the sections were permeabilized with 0.1% Triton X-100 in PBS at room temperature for 10 min. The sections were then blocked with 5% normal goat serum (Beyotime Institute of Biotechnology) at room temperature for 1 h to reduce non-specific binding, and endogenous peroxidase activity was quenched by incubating the sections in 3% hydrogen peroxide in methanol at room temperature for 10 min. The sections were then incubated with the following primary antibodies (1:200): Ki-67 (cat. no. A20018; ABclonal Biotech Co., Ltd.), E-cadherin (cat. no. 20874-1-AP; Proteintech Group, Inc.), Vimentin (cat. no. 5741; Cell Signaling Technology, Inc.) CD69 (cat. no. A26620PM; ABclonal Biotech Co., Ltd.), CD11c (cat. no. 17342-1-AP; Proteintech Group, Inc.) at 4˚C overnight. After washing the sections three times with PBS (5 min each), they were incubated with secondary antibodies (1:500): HRP-conjugated goat anti-rabbit IgG (H+L) (cat. no. AS014; ABclonal Biotech Co., Ltd.) and HRP-conjugated rabbit anti-mouse (cat. no. AS115; ABclonal Biotech Co., Ltd.) secondary antibodies at room temperature for 1 h.

For H&E staining, the sections were stained with hematoxylin for 5 min at room temperature, washed with running tap water for 5 min, then differentiated in 1% acid alcohol for a few seconds, washed again, and blued in Scott's tap water substitute for 2 min. Subsequently, the sections were stained with eosin Y solution (1% eosin in water) for 3 min at room temperature. The stained sections were observed under a light microscope. Images of H&E staining and IHC were captured using an IX71 inverted microscope (Olympus Corporation) and analyzed using ImageJ software.

TUNEL assay. Tumor tissues were fixed in 10% neutral buffered formalin at room temperature for 24 h, embedded in paraffin and sectioned (4 μm). After deparaffinization and antigen retrieval with 20 μg/ml proteinase K at 37˚C for 30 min, apoptosis was detected using the *In Situ* Cell Death Detection Kit (Roche Diagnostics). The sections were incubated with TUNEL reaction mix at 37˚C for 1 h, followed by incubation with a peroxidase-conjugated anti-fluorescein antibody at 37˚C for 30 min, and DAB chromogenic development for 10 min. Nuclei were counterstained with hematoxylin, and the sections were dehydrated and mounted. Positive (DNase I pretreatment) and negative (TdT omission) controls were included. Images were captured using an IX71 inverted light microscope (Olympus Corporation). For each sample, a total of three fields of view were randomly selected and imaged. Subsequently, these images were analyzed using ImageJ software.

RNA sequencing. Total RNA was extracted from tumor tissues using the RNA purification kit (cat. no. EZB-RN4; EZBioscience), and the concentration and purity of the extracted RNA were measured using a Nanodrop 2000 (Thermo Fisher Scientific, Inc.). The integrity of the RNA was assessed by agarose gel electrophoresis and the RNA quality number value was determined using an Agilent 5300 (Agilent Technologies, Inc.). The requirements for RNA sequencing were a total RNA amount of 1 μg, a concentration ≥30 ng/μl, and an OD260/280 ratio between 1.8 and 2.2. Sequencing was performed on an Illumina NovaSeq 6000 (Illumina, Inc.). Paired-end sequencing with 150 bp reads was carried out. The final library concentration was measured by qPCR with the KAPA Library Quantification Kit (Roche Diagnostics) and diluted to 1.8 pM. Raw data were converted to FASTQ by bcl2fastq v2.20 (Illumina, Inc.). Quality was assessed by FastQC v0.11.9 (https://www.bioinformatics.babraham.ac.uk/projects/fastqc/). Gene expression was quantified by featureCounts (http://subread.sourceforge.net/; version2.0.3), and differential expression analysis was performed using DESeq2 (http://bioconductor.org/packages/release/bioc/html/DESeq2.html; version 1.34.0). Log2 fold change (FC) >1.2 and P<0.05 were used to identify differentially expressed genes (DEGs) between model and Cur groups. Gene Ontology (GO) and Kyoto Encyclopedia of Genes and Genomes (KEGG) pathway analyses were performed using the clusterProfiler R package (https://bioconductor.org/packages/clusterProfiler; version 4.4.4), referencing the KEGG database (https://www.kegg.jp; version 107.0).

Gene set enrichment analysis (GSEA). Gene expression data from RNA sequencing were collected for both the model group and the Cur group. To conduct GSEA, gene sets from the Molecular Signatures Database (MSigDB) (https://www.gsea-msigdb.org/gsea/msigdb/index.jsp) were initially sourced. Subsequently, the analysis was run on GSEA software (https://www.gsea-msigdb.org/gsea/downloads.jsp). The results were interpreted via enrichment score (ES), normalized enrichment score (NES) and P-value.

Comparative analysis of human and mouse solute carrier family 7 member 11 (SLC7A11) proteins. To assess potential species-specific differences in SLC7A11, a comparative analysis of the protein sequences and structures between humans and mice was performed. The amino acid sequences of human SLC7A11 (UniProt ID: Q9UPY5) and mouse SLC7A11 (UniProt ID: Q9WTR6) were retrieved from the UniProt database (https://www.uniprot.org/). Sequence alignment and identity calculations were conducted using Clustal Omega (http://www.clustal.org/omega/; version 1.2.4), with a focus on functionally critical domains (e.g., substrate-binding sites, transmembrane helices). Three-dimensional (3D) structural predictions were generated using the AlphaFold database (https://alphafold.ebi.ac.uk/) (human: AF-Q9UPY5-F1; mouse: AF-Q9WTR6-F1) and structural similarity was evaluated using PyMOL (https://pymol.org/; version 2.1).

Molecular docking. For molecular docking, the Cur compound was used as a small-molecule ligand with SLC7A11 protein targets as receptors. The target protein structures of SLC7A11 (UniProt ID: Q9WTR6) were obtained from the UniProt database and the Royal Society of Chemistry Database (https://www.chemspider.com). The center positions of the grid box were determined on the basis of the interaction between the small molecule and target (x=-1.873, y=-6.83, z=10.886). The coordinates represent the center of the grid box used for molecular docking simulations. This grid box was defined to encompass the binding site of the target protein, where the small molecule interacts with key residues. The center position was determined based on the centroid of the co-crystallized ligand or by aligning the target structure with known active site coordinates from homologous proteins. Molecular docking was then performed in batches with AutoDock Vina (https://github.com/ccsb-scripps/AutoDock-Vina; version 1.2.5). Using PyMOL 2.1 software, irrelevant small molecules were removed from the protein structures. Water molecules were removed and hydrogen atoms were added after the proteins were imported into AutoDock Tools 1.5.6 (http://mgltools.scripps.edu/downloads/). Finally, the structures were converted into pdbqt files. Molecular docking calculations utilized the Lamarckian genetic algorithm (15), configured with a population size of 150 individuals, a cap of 25 million energy evaluations, a generation limit of 2,000, a crossover rate set at 0.8, a mutation rate of 0.02, and 100 separate docking runs. Binding free energy served as the criterion for assessing the final docking structures.

Survival analysis. Survival analysis was performed using breast cancer tissue data from The Cancer Genome Atlas in the Gene Expression Profiling Interactive Analysis 2 database (http://gepia2.cancer-pku.cn/#index). The quartile method (which divides a dataset into four equal parts) was used to categorize the SLC7A11 gene expression levels in the samples. The association between gene expression and DFS was analyzed through log-rank test, and a Kaplan-Meier curve was generated to visually represent the DFS rates for different groups based on gene expression levels (cutoff: High expression group, 75%; low expression group, 25%).

Reverse transcription-quantitative polymerase chain reaction (RT-qPCR). RNA was extracted from tumor tissues using TRIzol® (Invitrogen; Thermo Fisher Scientific, Inc.) and RT was performed using the RT kit according to the manufacturer's protocol (Accurate Biology, Inc.). The resultant cDNA underwent qPCR under the following conditions: Initial cycle at 95˚C for 60 sec, followed by 40 cycles of denaturation at 95˚C for 15 sec, annealing at 60˚C for 15 sec and extension at 72˚C for 45 sec. qPCR was performed using the SYBR Green Master Mix (Takara Bio, Inc.). The housekeeping gene used was β-actin. The mRNA expression levels were quantified using the QuantStudio Real-time PCR System (Applied Biosystems; Thermo Fisher Scientific, Inc.). The primer sequences corresponding to the target genes are provided in Table I. The $2^{-\Delta\Delta Cq}$ method was used to analysis relative gene expression data (16).

Lipid reactive oxygen species (ROS) assay. MDA-MB-231 cells were plated in 6-well dishes at a density of $3x10^6$ cells/well, and were exposed to 100 μM Cur and/or 10 μM Fer-1 for 24 h at 37˚C. After 24 h, the culture medium was substituted with 2 ml fresh medium containing 5 μM BODIPY-C11 (Thermo

Table I. Sequences of the primers used in reverse transcription-quantitative polymerase chain reaction analysis.

Gene	Sequence, 5'-3'
Mouse IL7	Forward: TCGTGCTGCTCGCAAGTTG
	Reverse: CTTGTGCAGTTCACCAGTGTTTG
Mouse HCAR2	Forward: GGACAGACATGCCAAGATCAAG
	Reverse: CCAGGTCCACCGAGGAGTAG
Mouse NF-κBID	Forward: TCCCCACAGTTGCCTTCAC
	Reverse: GAGCGTGTCTCCTTCCTCATC
Mouse SLC7A11	Forward: GCTATCATCACAGTGGGCTACG
	Reverse: GGGCAACAAAGATCGGGAC
Mouse APLNR	Forward: CGGCTAAGGCTGCGAGTC
	Reverse: CTGGATCTTGGTGCCATTTTC
Mouse TGF-β	Forward: TCGACATGGATCAGTTTATGCG
	Reverse: CCCTGGTACTGTTGTAGATGGA

APLNR, angiotensin receptor like 1; HCAR2, hydroxycarboxylic acid receptor 2; SLC7A11, solute carrier family 7 member 11.

Fisher Scientific, Inc.) and incubated at 37˚C for 30 min in the dark. Subsequently, the cells were washed with PBS to eliminate any excess dye after harvesting. Flow cytometry was performed using a BD FACSCanto II flow cytometer (BD Biosciences) to examine the levels of lipid ROS stained with BODIPY-C11. Data were analyzed using FlowJo software (version 10.8; BD Biosciences). The experiment was independently repeated three times.

2',7'-Dichlorodihydrofluorescein diacetate (DCFH-DA) assay. 4T1 and MDA-MB-231 cells were seeded in confocal-suitable dishes at a density of $3x10^6$ cells/well, then exposed to 100 μM Cur for 24 h at 37˚C. After washing with serum-free medium, the cells were incubated with 10 μM DCFH-DA (Beyotime Institute of Biotechnology) for 30 min. Subsequently, the cells were washed again to remove excess probe. Samples were observed under a confocal laser scanning microscope. DCF was excited at 488-495 nm and its emission was collected at 510-530 nm. The images were captured using a confocal laser scanning microscope (Zeiss AG).

Statistical analysis. Data are presented as the mean ± SD from three independent experiments. All statistical analyses were performed using SPSS Statistics (version 28.0; IBM Corp.). Normality and homogeneity of variances were confirmed using Shapiro-Wilk and Levene's tests, respectively. Statistical differences among groups were analyzed by one-way analysis of variance (ANOVA), followed by Tukey's honestly significant difference post hoc test for pairwise comparisons when ANOVA indicated significant overall effects ($P<0.05$). Two-tailed $P<0.05$ was considered to indicate a statistically significant difference.

Results

Cur inhibits the viability, migration, invasion and colony formation of TNBC cells. The 4T1 and MDA-MB-231 cell lines were used to conduct CCK-8 assays and to investigate the effects of Cur on the viability of TNBC cells. Treatment with multiple doses of Cur (0, 6.25, 12.5, 25, 50, 100, 200 and 400 μM) (Fig. 2A) for 24 and 48 h decreased the viability of TNBC cells ($P<0.05$; Fig. 2B). The IC_{50} values for Cur intervention in TNBC cells after 24 h were 98.76 and 190.2 μM, and the IC_{50} values for Cur intervention after 48 h were 95.11 and 169.8 μM. Subsequently, experiments were conducted using Cur concentrations of 25, 50 and 100 μM. To elucidate the impact of Cur on the sensitivity of TNBC cells to PTX, a series of additional experiments were executed. After 24 h of intervention, Cur at concentrations of 50 and 100 μM exerted a marked effect on enhancing the sensitivity of both 4T1 and MDA-MB-231 cells to 50 nM PTX ($P<0.05$; Fig. 2C). In addition, the sensitivity to 500 nM PTX was significantly increased by the presence of 50 and 100 μM Cur in MDA-MB-231 cells ($P<0.05$), and by 100 μM Cur in 4T1 cells ($P<0.05$). These findings provided crucial insights into the potential combined application of Cur and PTX in the treatment of TNBC. Furthermore, treatment with Cur (50 and 100 μM) inhibited the migration rate of 4T1 and MDA-MB-231 cells after intervention for 24 h ($P<0.05$; Fig. 2D). The Transwell assay results indicated that Cur (25, 50, and 100 μM) significantly decreased the invasive abilities of 4T1 and MDA-MB-231 cells ($P<0.01$; Fig. 2E). In addition, colony formation abilities were significantly reduced in the 25, 50, and 100 μM Cur-treated groups ($P<0.05$; Fig. 2F). Taken together, these results indicated that Cur may significantly inhibit the survival of TNBC cells *in vitro*.

Cur regulates the expression of apoptosis-associated proteins and EMT of TNBC cells. Next, WB was performed to observe the effects of Cur on the expression of apoptosis-associated proteins in TNBC cells. The results showed that, after 24 h of intervention with 100 μM Cur in 4T1 and MDA-MB-231 cells, the expression levels of the proapoptotic proteins cleaved caspase 9, cleaved caspase 3 and BAX were increased, whereas those of the antiapoptotic protein BCL-2 were significantly inhibited ($P<0.05$; Fig. 3A). The dual bands of BCL-2 may reflect its known post-translational modifications or splice variants in TNBC cells. Antibody specificity was ensured via a positive control and consistent sample processing, and the loading controls confirmed equal protein loading without degradation. EMT is tightly linked to the invasion and metastasis of tumors, and is mainly distinguished by the lack of E-cadherin, along with the increased expression levels of N-cadherin and Vimentin (15). Therefore, the current study examined the protein levels of E-cadherin, N-cadherin and Vimentin. It was revealed that 24 h of intervention with 100 μM Cur could upregulate the protein expression levels of E-cadherin, and downregulate those of N-cadherin and Vimentin ($P<0.05$; Fig. 3B). Immunofluorescence experiments revealed that the protein expression of E-cadherin was markedly elevated (green), whereas that of Vimentin was decreased (red) following treatment with 100 μM Cur for 24 h (Fig. 3C). These results indicated that Cur may exert an inhibitory effect on the occurrence and development of EMT in TNBC cells.

Cur suppresses the growth and EMT of TNBC in vivo. A TNBC mouse model was established by subcutaneously injecting 4T1 cells into BALB/c mice to observe the anti-TNBC effects of Cur

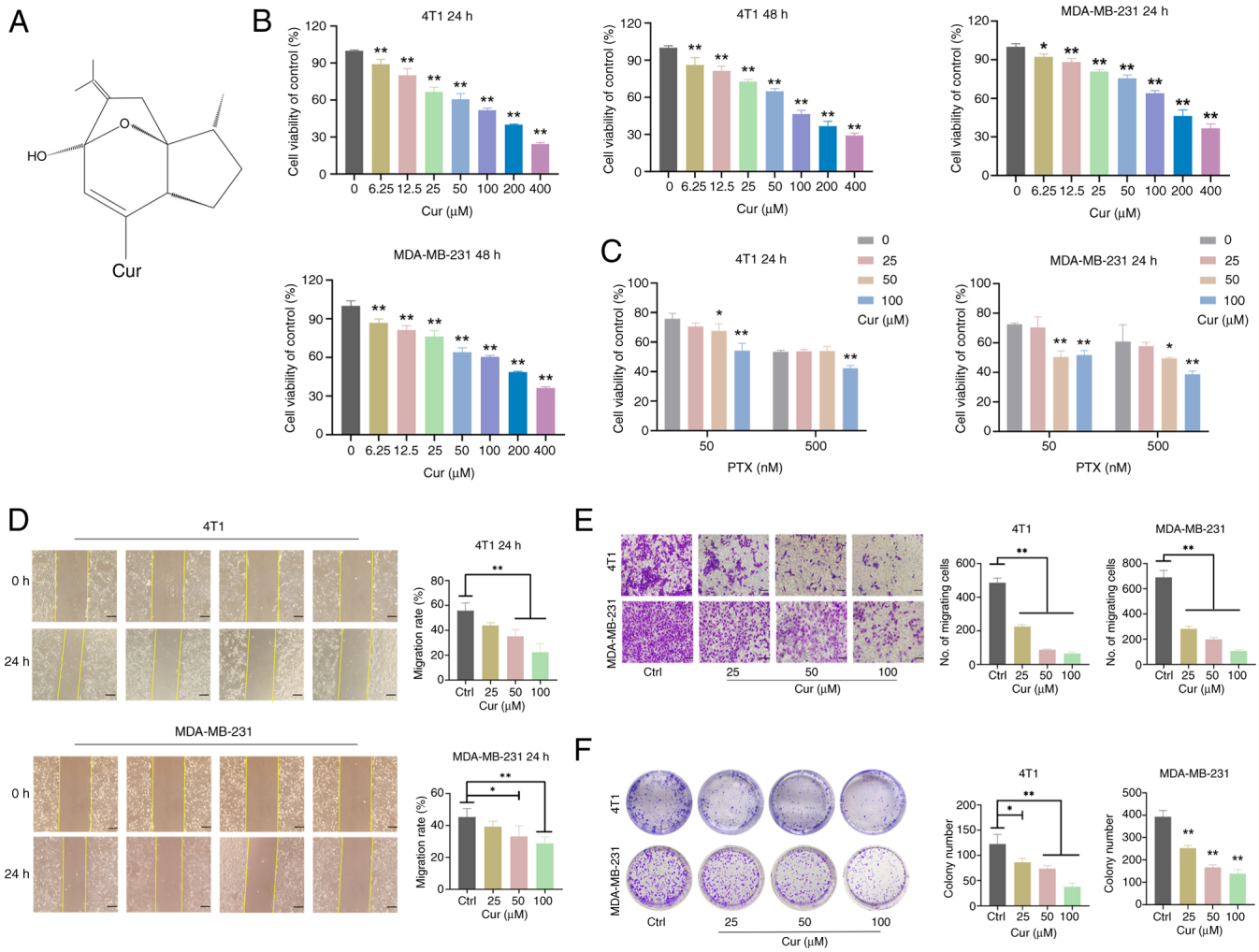

Figure 2. Effects of Cur on the viability, migration, invasion and colony formation of triple-negative breast cancer cells. (A) Chemical structure of Cur. (B) Viability of 4T1 and MDA-MB-231 cells treated with 6.25, 12.5, 25, 50, 100, 200 and 400 μM Cur for 24 and 48 h detected by CCK-8 assay. (C) Effects of 0, 25, 50 and 100 μM Cur, and 50 and 500 nM PTX on cell viability, as detected by CCK-8 assay. (D) Wound healing assays were performed to analyze cell migration after 4T1 and MDA-MB-231 cells were treated with 25, 50 and 100 μM Cur for 24 and 48 h. Scale bar, 100 μm. (E) Transwell assays were performed to evaluate cell invasion after 4T1 and MDA-MB-231 cells were treated with 25, 50 and 100 μM Cur for 24 h. Scale bar, 200 μm. (F) Colony formation assay of 4T1 and MDA-MB-231 cells grown for 7-10 days in the presence of the indicated concentrations of Cur or Ctrl. Data are presented as the mean ± SD (n=3). *P<0.05, **P<0.01 vs. Ctrl group or as indicated. CCK-8, Cell Counting Kit-8; Ctrl, control; Cur, curcumenol; PTX, paclitaxel.

(Fig. 4A). Compared with in the model group, Cur (10 mg/kg, every other day) or PTX (10 mg/kg/week) significantly inhibited the growth of TNBC xenograft tumors (Fig. 4B), as evidenced by dampened increases in tumor volume after 3 weeks of treatment (P<0.05; Fig. 4C). The maximum tumor volume observed in mice at the study endpoint was 2,407 mm^3, and the largest tumor diameter recorded was 17.3 mm. These values were carefully monitored and did not exceed the predefined ethical thresholds of 20 mm in diameter or 10% of body weight. Subsequently, the levels of proliferation and apoptosis markers were measured in tumor tissues. The results of IHC revealed that Cur treatment markedly suppressed Ki-67 expression in tumor tissues and induced apoptosis in tumor cells when compared with the model group (P<0.01; Fig. 4D). Furthermore, Cur significantly downregulated the expression levels of BCL-2, but significantly upregulated those of cleaved caspase 9, cleaved caspase 3 and BAX (P<0.05; Fig. 4E). Compared with in the model group, treatment with Cur could also inhibit the expression levels of N-cadherin and Vimentin, while increasing those of E-cadherin. These results revealed that Cur may regulate the apoptosis and EMT of TNBC tumors.

Cur alleviates TNBC lung metastasis in a mouse xenograft model. Given the potent lung metastatic properties of 4T1 cells (17), lung metastasis was also examined. The results showed that Cur and PTX could reduce the number of lung metastatic nodules in mice (Fig. 5A and B). In addition, H&E staining revealed that the lung metastatic lesion area was decreased after treatment with different doses of Cur or PTX (Fig. 5C). Furthermore, IHC results demonstrated that in metastatic lung tissue, Cur significantly upregulated E-cadherin levels, but downregulated Vimentin levels (P<0.01; Fig. 5D). In summary, Cur may regulate EMT marker proteins in lung metastatic lesions.

RNA sequencing analysis of the potential mechanisms of Cur in the treatment of TNBC. RNA sequencing was conducted

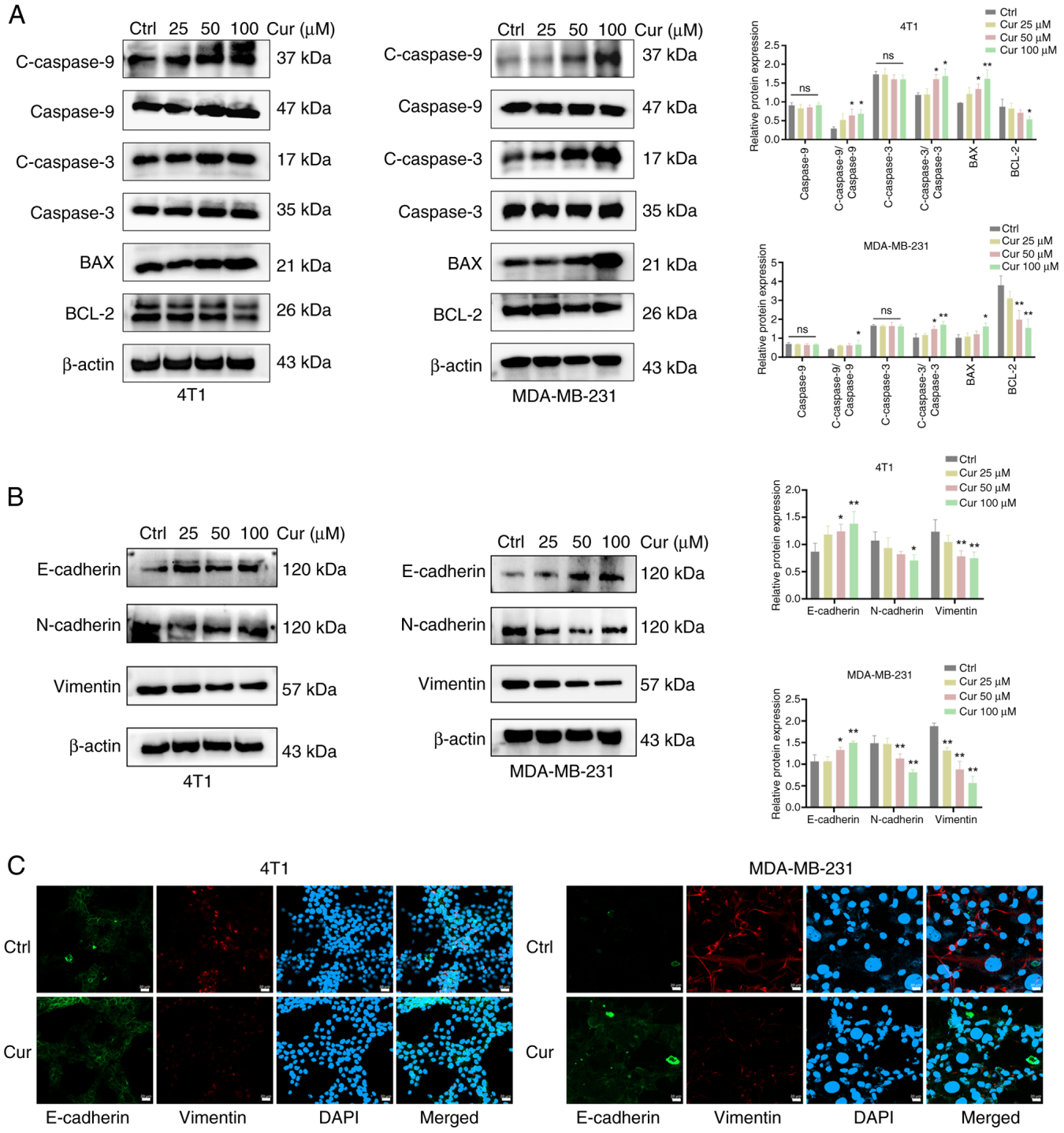

Figure 3. Effects of Cur on the apoptosis and epithelial-mesenchymal transition of triple-negative breast cancer cells. (A) Western blot analysis was performed to detect the protein expression levels of C-caspase 9, C-caspase 3, BAX and BCL-2 in 4T1 and MDA-MB-231 cells following treatment with the indicated concentrations of Cur or Ctrl for 24 h. (B) Protein expression levels of E-cadherin, N-cadherin and Vimentin in 4T1 and MDA-MB-231 cells following treatment with the indicated concentrations of Cur or Ctrl for 24 h. (C) Immunofluorescence staining of E-cadherin (green) and Vimentin (red) in 4T1 and MDA-MB-231 cells treated with 100 μM Cur or Ctrl for 24 h. Scale bar, 20 μm. Data are presented as the mean ± SD (n=3). *P<0.05, **P<0.01 vs. Ctrl group. C-, cleaved; Ctrl, control; Cur, Curcumenol; ns, not significant.

to analyze DEGs with log2 FC >1.2 and P<0.05. The results revealed that Cur upregulated 200 genes and downregulated 289 genes in TNBC tumor tissues (Fig. 6A and B). KEGG enrichment analysis showed that DEGs were enriched in the 'NF-kappa B signaling pathway', 'TGF-beta signaling pathway' and 'ferroptosis' (Fig. 6C) signaling pathways. GO analysis was used to classify the biological functions of Cur-related DEGs. These biological functions included 'actin filament-based process', 'cytoskeletal protein binding', 'multicellular organismal process' and 'biological regulation' (Fig. 6D).

Among the DEGs, SLC7A11 (P=0.032, log2 FC=-1.75), angiotensin receptor like 1 (APLNR; P=1.44x10^{-5}, log2 FC=-1.09), TGF-β2 (P<0.001, log2 FC=-1.24), IL7

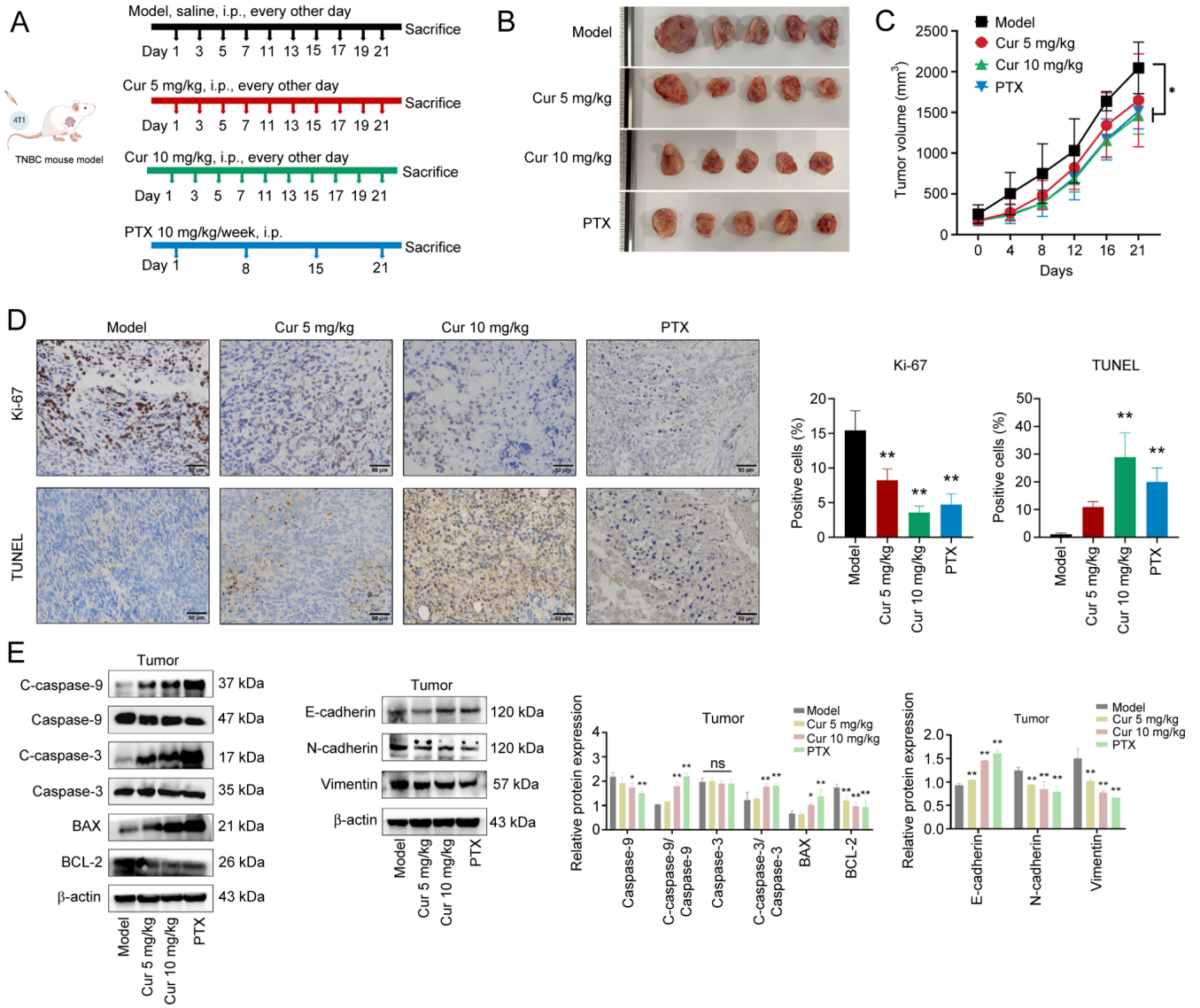

Figure 4. Effects of Cur on TNBC tumor growth *in vivo*. (A) Schematic diagram of the *in vivo* study on antitumor effects. (B) Representative images of tumors in different groups of 4T1-induced TNBC mouse models. (C) Tumor volumes of mice after treatment for 3 weeks. (D) Levels of Ki-67 and TUNEL in tumor tissues were determined using immunohistochemistry, which aimed to measure proliferation and apoptosis in the 4T1-induced TNBC mouse model. Scale bar, 50 μm. (E) Western blot analysis was performed to detect the protein expression levels of C-caspase 9, C-caspase 3, BAX, BCL-2, E-cadherin, N-cadherin and Vimentin. Data are presented as the mean ± SD (n=3). *P<0.05, **P<0.01 vs. Model group or as indicated. Cur, curcumenol; TNBC, triple-negative breast cancer; PTX, paclitaxel.

(P=3.57x10^{-8}, log2 FC=1.39), hydroxycarboxylic acid receptor 2 (HCAR2; P=2.51x10^{-5}, log2 FC=1.80) and NF-κBID (P<0.001, log2 FC=1.20) were regulated by Cur. The effects of Cur on the mRNA expression levels of SLC7A11, APLNR, TGF-β, IL7, HCAR2 and NF-κBID were verified in TNBC tumor tissues using RT-qPCR to validate the results of RNA sequencing. Consistent with the results of RNA sequencing, the mRNA expression levels of IL7, HCAR2 and NF-κBID were increased, whereas those of APLNR, SLC7A11 and TGF-β were decreased in the tumor tissues of mice following Cur (10 mg/kg) intervention (P<0.05; Fig. 6E).

On the basis of the normalized NESs obtained through the GSEA of the transcriptome sequencing results, it was revealed that Cur could significantly activate immune-related pathways, including 'antigen processing and presentation' (NES=2.06, P<0.001), the 'IL-17 signaling pathway' (NES=1.74, P<0.001), 'Th1 and Th2 cell differentiation' (NES=1.68, P<0.001), and 'Th17 cell differentiation' (NES=1.61, P<0.001) (Fig. 6F).

Antigen processing and presentation are vital processes for the immune system to recognize antigens and initiate an immune response. After antigens are internalized by cells, they bind to major histocompatibility complex molecules and are presented on the cell surface for T-cell recognition, thereby activating effective antitumor T-cell activity (18). Under stimulation by different cytokines and antigen signals, CD4^{+} T cells differentiate into helper T cells (Th cells). The generation of the Th1 effector subset depends on IL-12 and IFN-γ cytokines (19). Th2 cell immunity can permanently convert high-grade breast tumors into low-grade, fibrocystic-like structures (20). Th17 cells are a subset of CD4^{+} T cells, which mainly secrete cytokines, such as IL-17; notably, IL-17 and Th17 cells form a positive feedback loop, enhancing barrier

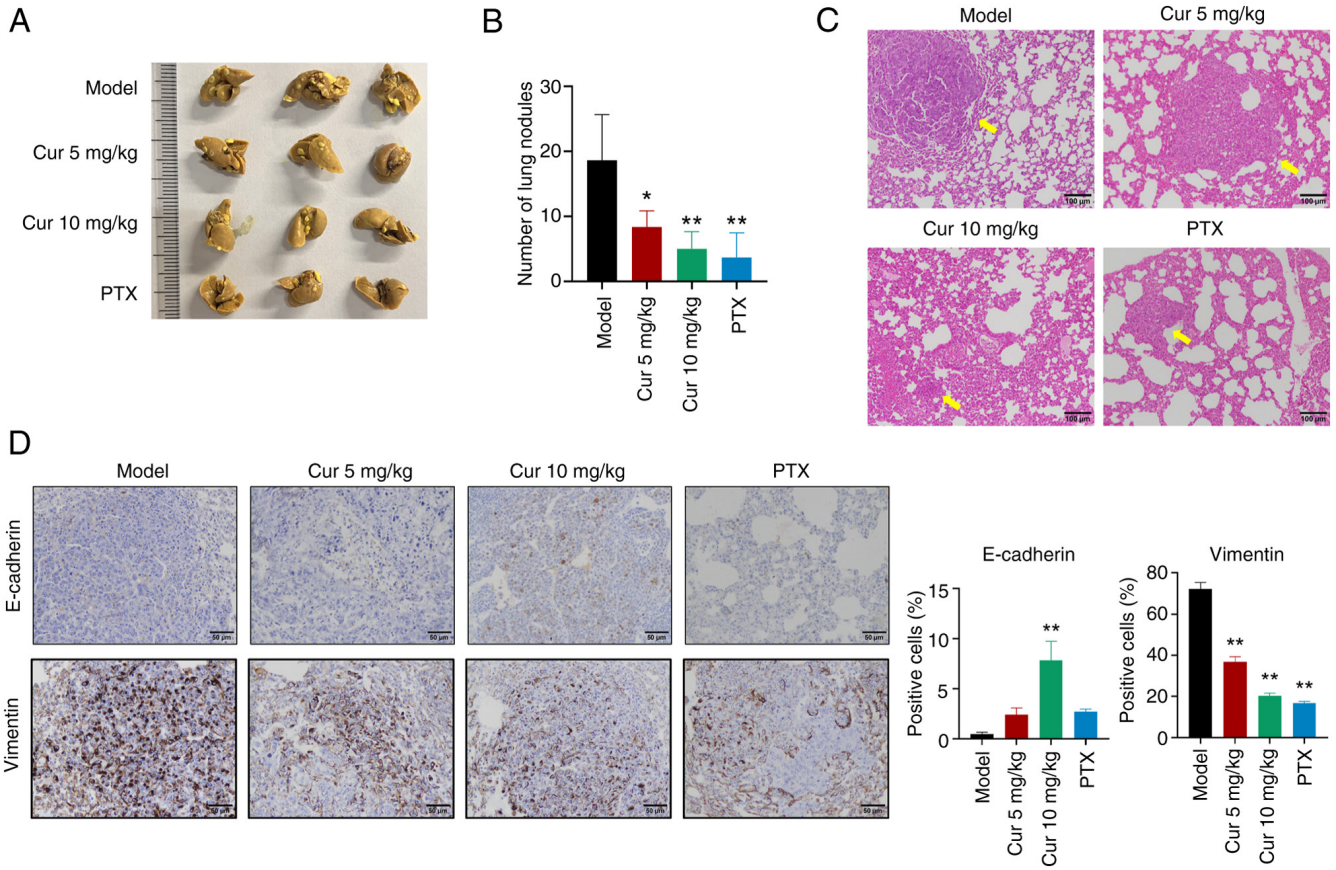

Figure 5. Cur alleviates triple-negative breast cancer lung metastasis in a mouse xenograft model. (A) Representative images of lung nodule images after Bouin's fixative solution and (B) lung nodule counts. (C) Hematoxlyin and eosin staining images of lung metastasis tissues from each group of mice. Scale bar, 100 μm. The arrows indicate lung metastases. (D) Protein expression levels of E-cadherin and Vimentin in lung metastatic lesions determined using immunohistochemistry. Scale bar, 50 μm. Data are presented as the mean ± SD (n=3). *P<0.05, **P<0.01 vs. Model group. Cur, curcumenol; PTX, paclitaxel.

immunity (21,22). In accordance with the current GSEA results, it could be hypothesized that Cur exerts a regulatory effect on dendritic cells (DCs) and CD4 cells in the tumor immune microenvironment. IHC results indicated that Cur could increase the expression levels of the DC-specific marker CD11c and promote the expression of the T-cell activation marker CD69 in mouse tumor tissues (P<0.01) (Fig. 6G).

Cur inhibits TNBC by modulating ferroptosis-related proteins. The downregulation of SLC7A11, a specific amino acid transporter, can inhibit the cysteine metabolism pathway, leading to reduced intracellular cystine levels and GSH biosynthesis depletion, indirectly inhibiting the activity of GPX4, subsequently causing lipid peroxide accumulation and ultimately inducing ferroptosis in cells (23). Ferroptosis represents a controlled type of cell death that occurs due to the buildup of lipid ROS, which are closely associated with oxidative stress responses and cysteine metabolism; it is the consequence of iron-dependent lipid peroxide accumulation (24,25). The results of the present molecular docking analysis indicated that Cur exhibited excellent binding capacity and compatibility with SLC7A11, with binding energies of -6.170 kcal/mol. Cur was revealed to form hydrogen bond interactions with the amino acid LEU-144 at the active site of the SLC7A11 protein, which is of importance to the ligand molecules in the active pocket of the anchor protein (Fig. 7A). Furthermore, this compound was revealed to form favorable hydrophobic interactions with ILE-165, PHE-146, LEU-385, LEU-144, VAL-141, ALA-145, ILE-64 and TYR-149, making an important contribution to the stabilization of small molecules. To explore potential species-specific differences in SLC7A11, a comparative analysis of the protein sequences and structures of SLC7A11 was performed in mice and humans. The amino acid sequences of human SLC7A11 (UniProt ID: Q9UPY5) and mouse SLC7A11 (UniProt ID: Q9WTR6) showed a high degree of amino acid sequence identity according to UniProt. In addition, the AlphaFold prediction model was used for 3D structure prediction, and the comparison of human SLC7A11 (AF-Q9UPY5-F1) with mouse SLC7A11 (AF-Q9WTR6-F1), and the overall 3D conformations were revealed to be highly similar (root mean square deviation=0.36) by PyMOL (Fig. 7B). These findings indicated there is a high degree of similarity and reproducibility in the regulatory mechanisms of Cur between humans and mice.

Bioinformatics analysis revealed that patients with breast cancer with low SLC7A11 expression had a longer DFS (HR=1.7, log-rank P=0.044) (Fig. 7C) than those without. WB revealed that in mouse tumor tissues, Cur could downregulate the protein expression levels of the ferroptosis inhibitors SLC7A11 and GPX4, whereas it promoted the protein expression levels of ACSL4, which facilitates lipid metabolism conducive to ferroptosis (Fig. 7D).

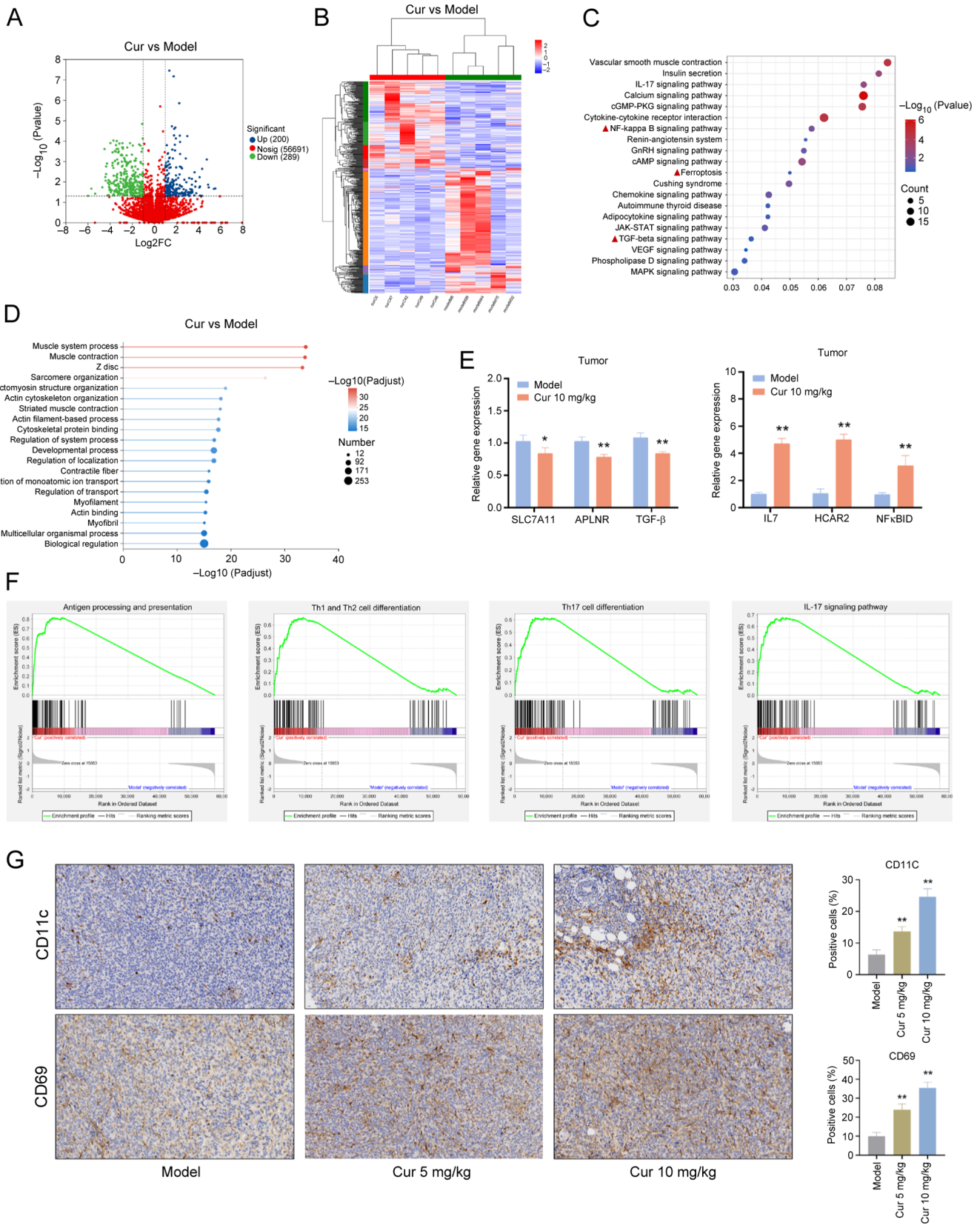

Figure 6. Identification of Cur-regulated candidate target genes in TNBC tumor tissues by RNA sequencing. (A) Volcano plots and (B) heatmap of upregulated and downregulated genes in tumor tissues from the Cur group compared with the model group (n=5). (C) Kyoto Encyclopedia of Genes and Genomes pathway enrichment analysis. (D) GO annotation analysis of differentially expressed genes. (E) Effect of Cur on SLC7A11, APLNR, TGF-β, IL7, HCAR2 and NF-κBID in TNBC tumor tissues determined using reverse transcription-quantitative polymerase chain reaction. (F) Gene Set Enrichment Analysis. (G) Immunohistochemistry was performed to detect the expression of CD11b (dendritic cell marker) and CD69 (T-cell activation marker) in each group of tumor tissues (magnification, x63). Data are presented as the mean ± SD (n=3). *P<0.05, **P<0.01 vs. Model group. APLNR, angiotensin receptor like 1; Cur, curcumenol; GO, Gene Ontology; HCAR2, hydroxycarboxylic acid receptor 2; SLC7A11, solute carrier family 7 member 11; TNBC, triple-negative breast cancer.

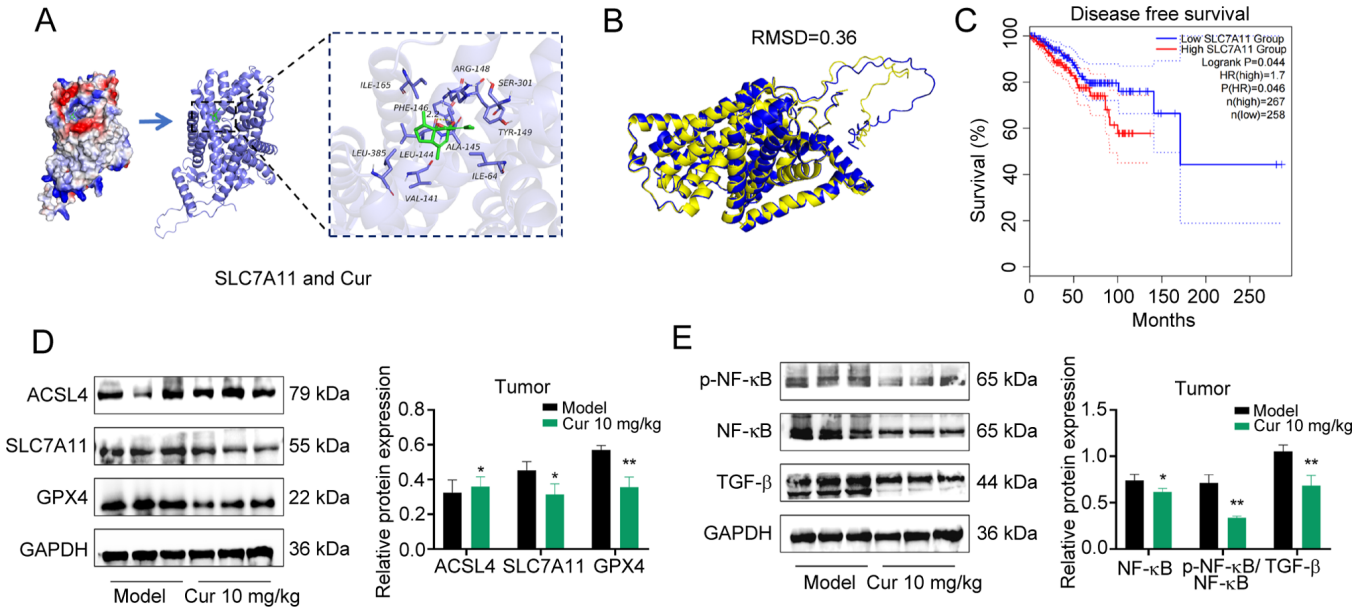

Figure 7. Cur inhibits TNBC by modulating ferroptosis-related proteins. (A) Molecular docking of Cur with SLC7A11. (B) 3D structure prediction and comparison of human SLC7A11 (yellow) with mouse SLC7A11 (blue) using AlphaFold and PyMOL. (C) Survival analysis of the association between SLC7A11 expression and disease-free survival in breast cancer. (D) Effect of Cur on the ferroptosis-related proteins SLC7A11, GPX4 and ACSL4 in tumors. (E) Effect of Cur on NF-κB and TGF-β protein expression, and p-NF-κB levels. Data are presented as the mean ± SD (n=3). *P<0.05, **P<0.01 vs. Model group. ACSL4, acyl-CoA synthetase long-chain family member 4; Cur, curcumenol; GPX4, glutathione peroxidase 4; p-, phosphorylated; SLC7A11, solute carrier family 7 member 11; RMSD, root mean square deviation.

As a member of the NF-κB kinase inhibitor family, NF-κBID, also known as inhibitor of NF-κB, serves as a key negative regulatory molecule of the NF-κB signaling pathway. NF-κBID can bind to NF-κB in the cytoplasm, thereby maintaining NF-κB in an inactivated state (26,27). TGF-β is a pivotal participant in regulating EMT in tumor cells and is one of the most important inducers of EMT (28); notably, the elevated expression of TGF-β is associated with accelerated EMT progression in tumors and adverse prognosis (29). Therefore, the current study detected the protein expression levels of NF-κB and TGF-β using WB. Consistent with our previous results, Cur could downregulate the phosphorylation of NF-κB and the protein expression levels of TGF-β in tumor tissues (P<0.05; Fig. 7E).

Cur can promote ferroptosis through the SLC7A11/NF-κB/TGF-β pathway. A reduction in mitochondrial membrane potential serves as a crucial characteristic of the mitochondrial-mediated apoptosis pathway. In ferroptotic cells, the mitochondrial membrane potential usually decreases, causing the fluorescence of JC-1 to shift from red to green (30). In the present study, treating TNBC cells with 100 μM Cur for 24 h resulted in the reduced aggregation of JC-1 in the mitochondrial matrix (red fluorescence) and increased expression of JC-1 monomers (green fluorescence); this finding indicated that the mitochondrial membrane potential was reduced after Cur treatment (Fig. 8A). The accumulation of ROS serves a pivotal role by promoting the generation of lipid peroxides during ferroptosis, subsequently driving the occurrence of ferroptosis. After 24 h of Cur intervention, 4T1 and MDA-MB-231 cells exhibited increased levels of ROS (Fig. 8B). Flow cytometry revealed that when Fer-1 was used to inhibit the occurrence of ferroptosis, the levels of lipid ROS were decreased compared with those in the control group; however, Cur was able to counteract the inhibitory effect of Fer-1 on ferroptosis (Fig. 8C). Similarly, Cur was shown to reduce the protein expression levels of SLC7A11 and GPX4 in MDA-MB-231 cells, while increasing those of ACSL4. Despite the presence of the ferroptosis inhibitor Fer-1, the intervention with Cur in the Fer-1 + Cur group could still downregulate the protein expression of SLC7A11 and GPX4, compared with those in the control group. This may imply that Cur could rescue the inhibitory effects of Fer-1 on ferroptosis in MDA-MB-231 cells (Fig. 8D). These data indicated that Cur could regulate ferroptosis and inhibit the malignant progression of cells in TNBC by inhibiting the SLC7A11/NF-κB/TGF-β signaling pathway.

Discussion

TNBC is the most challenging subtype of breast cancer to treat, which displays a high degree of invasiveness and metastatic potential. Tumor metastasis is a sophisticated biological process that involves EMT, enabling cells to penetrate the adjacent basement membrane, enter the circulatory system, travel to distant organs and ultimately lead to metastasis (31).

Emerging modes of tumor cell death, such as ferroptosis and disulfidptosis, have been discovered and are tightly regulated by the internal metabolic processes within tumors (32). The inhibition of voltage-dependent anion channel 3-derived circular RNA can elevate the levels of ROS, trigger the accumulation of the labile iron pool and subsequently induce ferroptosis in breast cancer cells. Consequently, this enhances the sensitivity of HER2-low breast cancer cells to trastuzumab deruxtecan treatment (33). SLC7A11, also known as xCT, is an important membrane protein that indirectly inhibits the

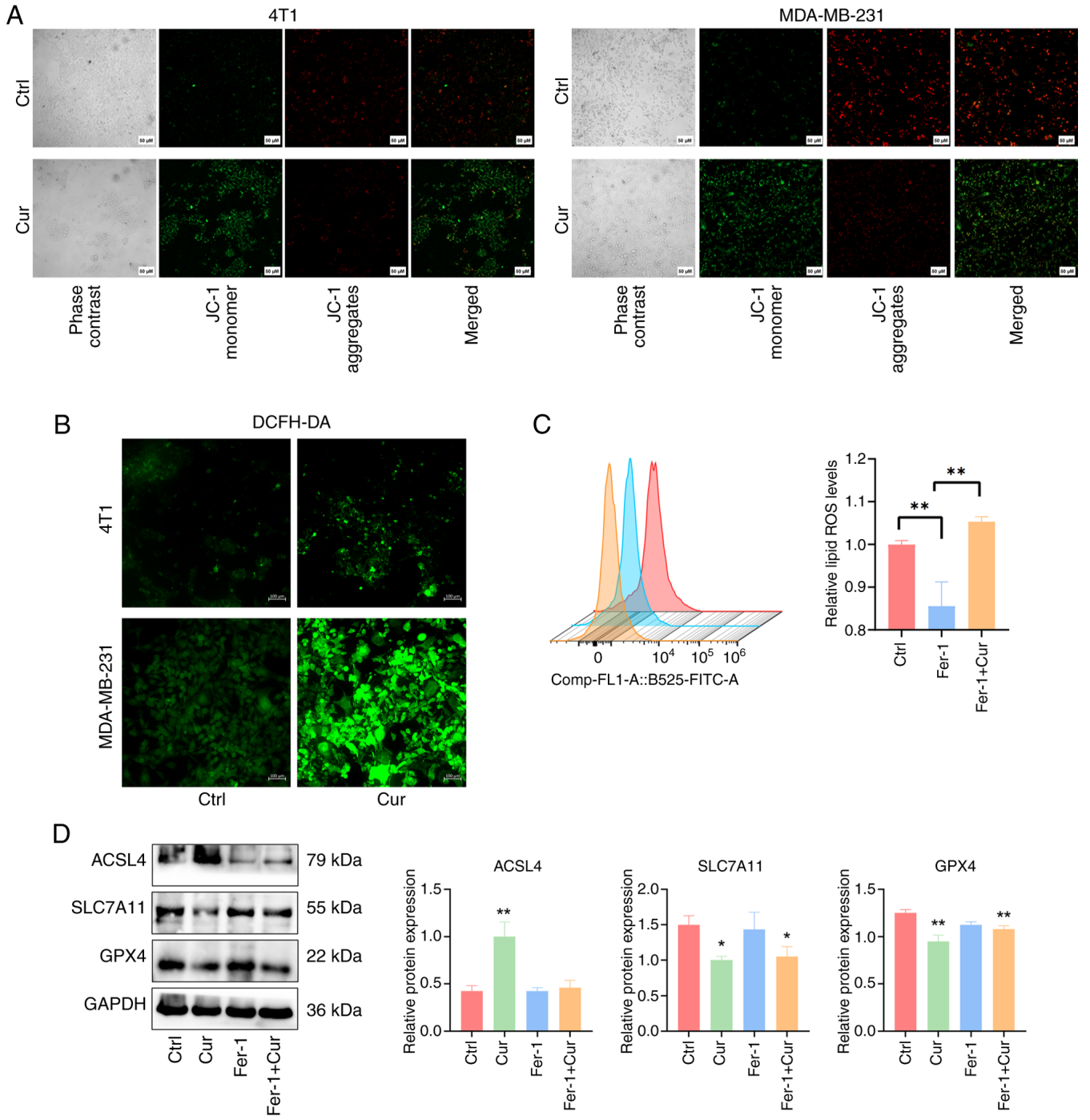

Figure 8. Cur can promote ROS accumulation and ferroptosis. (A) Fluorescence images of JC-1 aggregates (red) and JC-1 monomers (green) in 4T1 and MDA-MB-231 cells treated with 100 μM Cur or Ctrl for 24 h. Scale bar, 50 μm. (B) Labeling of 4T1 and MDA-MB-231 cells with the DCFH-DA fluorescent probe to assess the level of ROS release. Scale bar, 100 μm. (C) Flow cytometry of lipid ROS levels in MDA-MB-231 cells after 24 h of treatment with Fer-1 alone or in combination with Cur. (D) Western blot analysis was performed to detect the expression levels of the ferroptosis-related proteins SLC7A11, GPX4 and ACSL4 in MDA-MB-231 cells. Data are presented as the mean ± SD (n=3). *P<0.05, **P<0.01 vs. Ctrl group or as indicated. ACSL4, acyl-CoA synthetase long-chain family member 4; Ctrl, control; Cur, curcumenol; DCFH-DA, 2',7'-dichlorodihydrofluorescein diacetate; Fer-1, ferrostatin-1; GPX4, glutathione peroxidase 4; ROS, reactive oxygen species; SLC7A11, solute carrier family 7 member 11.

occurrence of ferroptosis by promoting GSH synthesis (34). Research has indicated that the NF-κB/SLC7A11 signaling pathway can regulate ferroptosis in mastitis (35). The transduction of the NF-κB pathway is well recognized to serve a crucial role in breast (36), colorectal (37), pancreatic (38) and cervical cancer (39). NF-κB serves as a biomarker for cancer staging, progression and prognosis, and its upregulation is associated with tumor progression in breast cancer (40,41). Furthermore, the interaction between the NF-κB and TGF-β signaling pathways has been extensively studied in various contexts, including cancer biology (42-44). NF-κB regulates the expression of TGF-β and inhibiting NF-κB could reduce the expression of TGF-β, enhancing the sensitivity of breast cancer cells to chemotherapeutic drugs (45). In neuroblastoma,

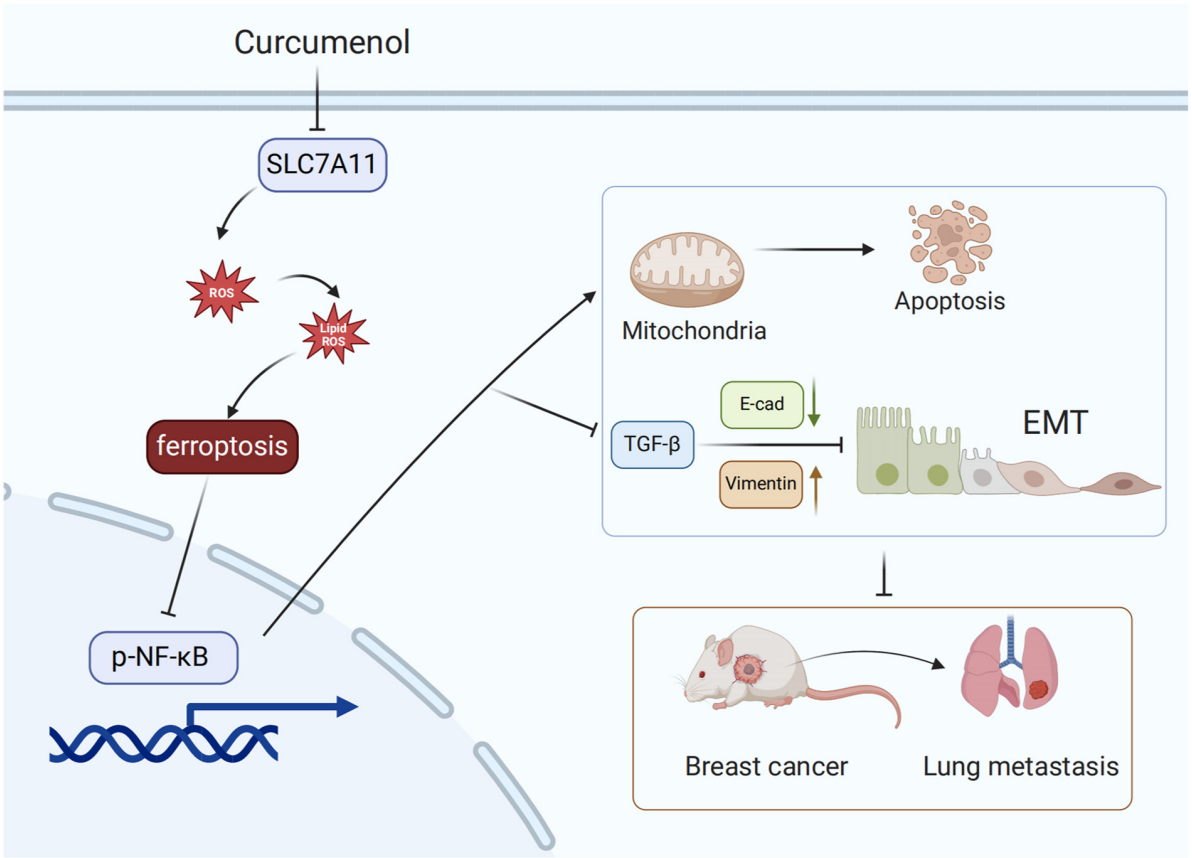

Figure 9. Potential mechanisms of Cur in the treatment of TNBC. Cur inhibits SLC7A11 expression, NF-κB and TGF-β signaling, and EMT, and promotes ROS accumulation and apoptosis in triple-negative breast cancer. Cur, curcumenol; E-cad, E-cadherin; EMT, epithelial-mesenchymal transition; p-, phosphorylated; ROS, reactive oxygen species; SLC7A11, solute carrier family 7 member 11.

the activation of TGF-β can activate the NF-κB pathway, regulating the tumor microenvironment and promoting the development of drug resistance (46).

A growing body of research has focused on utilizing natural products for cancer therapy, and *C. phaeocaulis* Valeton is a promising plant in this field. Compounds extracted from *C. phaeocaulis* Valeton exhibit high antitumor efficacy and safety in breast cancer (47). Treatment with *C. phaeocaulis* Valeton has been shown to inhibit the proliferation of MCF-7 cells by inducing apoptosis mediated by increased ROS formation, regulating the expression of BCL-2 family proteins and activating caspases (48). Furthermore, it has been demonstrated that curcumin can hinder the migration and invasion of breast cancer cells by suppressing cancer stem cell characteristics and EMT (49). Curcumin can also inhibit the formation of mammospheres, and downregulate the expression levels of E-cadherin and Vimentin (50). In liver cancer, curcumol has been demonstrated to inhibit cell proliferation by suppressing apoptosis and cell cycle arrest, while also inhibiting cell invasion and metastasis (51). Al-Amin *et al* (52) isolated bioactive compounds from *C. phaeocaulis* Valeton; comosone II was shown to inhibit the migration and invasion of MDA-MB-231 cells by suppressing matrix metalloproteinase-9.

While numerous bioactive compounds isolated from *C. phaeocaulis* Valeton have demonstrated antitumor potential across various types of cancer, to the best of our knowledge, the therapeutic efficacy of Cur against breast cancer remained unclear prior to the current study. This study systematically deciphered the multimodal inhibitory effects of Cur on TNBC progression through integrated mechanistic approaches. Consistent with the reported activities of other compounds in *C. phaeocaulis* Valeton, the present study indicated that Cur can inhibit the migration, invasion and EMT of TNBC cells, while promoting cell apoptosis.

In the malignant progression of tumors, EMT and ferroptosis exhibit an interactive relationship. Cancer cells undergo metabolic changes and may modify iron metabolism pathways to evade ferroptosis during EMT. For example, in cells undergoing EMT, the expression of iron-regulatory proteins (such as iron transporters and ferritin) is increased to avert lipid peroxidation and hinder the accumulation of free iron ions (53). It has also been found that 4-methoxydalbergione can inhibit tumorigenesis and metastasis in lung cancer by promoting ferroptosis (54). The present study indicated that Cur could regulate ferroptosis-related proteins and ROS accumulation in TNBC while inhibiting the occurrence of EMT; these effects may be interrelated. However, considering that excessive ROS levels have the potential to induce cell death, Cur may also promote the apoptosis of TNBC cells through the accumulation of ROS. By modulating the ROS-mediated EMT and apoptotic pathways, Cur may provide a promising therapeutic strategy for patients with TNBC, offering a novel perspective of targeted cancer therapy (55).

In the present study, the selection of Cur concentrations was determined based on both preliminary pharmacological assessments and established precedents in related research. For *in vitro* experiments, the chosen concentrations of 25, 50 and 100 μM were guided by the IC_{50} values of Cur in TNBC cells, and prior studies demonstrating that curcuminoids and structurally related compounds exhibit anti-migratory and anti-proliferative effects on cancer cells within this concentration range without inducing excessive cytotoxicity (56,57). Notably, 100 μM Cur exerted the most pronounced inhibitory effects on TNBC cells, aligning with the observed dose-dependent response. For *in vivo* studies, the doses of 5 and 10 mg/kg were selected to balance efficacy and safety, referencing previous work in colorectal and prostate cancer models where similar doses of Cur derivatives suppressed tumor growth and metastasis (58,59). While both doses reduced TNBC tumor burden, the 10 mg/kg dose demonstrated superior regulation of tumor proliferation, apoptosis and metastasis inhibition, suggesting its optimal therapeutic potential within a safe dosing window. Further studies are warranted to explore higher doses and refine pharmacokinetic parameters for clinical translation.

Notably, an interesting phenomenon emerged in the present study: Cur did not have completely identical inhibitory effects on the proliferation and migration of 4T1 and MDA-MB-231 cells. This finding is consistent with the results of other studies on breast cancer (60). The 4T1 cell line is known for its highly aggressive and metastatic behavior in murine models, characterized by rapid proliferation and robust invasiveness (61). By contrast, MDA-MB-231 cells, while also aggressive, may exhibit different metabolic dependencies that could modulate their response to Cur. For example, the high glutamine dependency of the redox homeostasis of 4T1 cells (linked to SLC7A11-mediated cystine uptake) might render them highly sensitive to Cur (62,63). Another interesting phenomenon was that the alterations in cleaved caspase 9/3 activation and BAX expression were observed only at higher Cur concentrations (50 or 100 μM), whereas lower doses (25 μM) showed minimal effects. This dose-dependent threshold phenomenon may arise from the cumulative disruption of pro-survival signaling required to overcome cellular apoptotic resistance. Moreover, the differential sensitivity between 4T1 and MDA-MB-231 cells can be ascribed to the basal expression levels of prosurvival proteins. MDA-MB-231 cells exhibit relatively elevated baseline levels of anti-apoptotic proteins, such as BCL-2. In future studies, in-depth molecular and genetic analyses could be conducted to elucidate the underlying mechanisms. Such analyses will not only improve the understanding of the effects of Cur on different cell lines, but could also contribute to the development of targeted cancer therapies.

Since 4T1 is a TNBC cell line characterized by high levels of lung metastasis, the current study further revealed that Cur could prevent lung metastasis in mice with primary tumors. In our previous study, TCM compound prescriptions, including *C. phaeocaulis* Valeton, have been shown to exert marked preventive effects against lung metastasis (64). Therefore, this finding suggested that Cur may indeed serve a crucial role in inhibiting the process of lung metastasis. Furthermore, it was discovered that Cur could inhibit the expression of APLNR. The APLNR signaling pathway can induce the secretion of angiogenesis factors, such as vascular endothelial growth factor, thus promoting tumor angiogenesis (65,66). The results of RT-qPCR verified the inhibitory effect of Cur on APLNR in tumor tissues, suggesting that vascular growth may also be a potential mechanism for Cur in the treatment of TNBC.

Although comprehensive research methods were employed, certain methodological drawbacks exist in the present study. Notably, 4T1 cells were used to establish an animal model of TNBC; while the use of 4T1 cells for modeling has been widely adopted, these cells exhibit certain differences from human breast cancer in terms of the tumor microenvironment, immune responses and heterogeneity. Future studies should consider using animal models developed from human-derived TNBC cells or patient-derived xenograft models to comprehensively elucidate the effects of Cur from multiple perspectives.

The present study demonstrated that Cur exerted inhibitory effects on the survival of TNBC cells *in vitro* and markedly suppressed their migration and invasion. Further experiments revealed that Cur could promote lipid ROS accumulation and regulate ferroptosis-related proteins. To the best of our knowledge, the present study is the first to reveal that Cur can markedly inhibit TNBC by decreasing the SLC7A11/NF-κB/TGF-β signaling pathway (Fig. 9).

Despite the potential of Cur for TNBC treatment, rigorously designed clinical trials are still needed for its clinical translation (67). Subsequent works should initially focus on completing pharmacokinetic and toxicological studies to evaluate the absorption, distribution, metabolism, excretion and toxicological characteristics of Cur. The solubility and stability of Cur remain to be further improved, and strategies, such as nanoparticle encapsulation or liposomal drug delivery systems, should be developed to optimize its formulation (68,69). Ensuring strict pharmaceutical supervision and quality control is particularly important. Finally, phase I clinical trials, with a focus on the safety and tolerability of Cur in patients with TNBC, need to be successively conducted. After ensuring the safety of Cur, clinical studies on the synergistic treatment of TNBC with Cur and chemotherapeutic drugs, such as PTX, or the prevention and treatment of TNBC lung metastasis must be planned. Overall, although existing research has demonstrated the anticancer effects of Cur, further studies are required to explore the potential use of Cur for the treatment of TNBC.

Acknowledgements

Not applicable.

Funding

This work was supported by the National Natural Science Foundation of China funded project (grant no. 82405389), the Postdoctoral Fellowship Program of China Postdoctoral Science Foundation (grant no. GZC20231706), and the Shanghai Post-doctoral Excellence Program (grant no. 2023547).

Availability of data and materials

The RNA sequencing data generated in the present study may be found in the National Centre for Biotechnology Information

under accession number PRJNA1233780 or at the following URL: https://www.ncbi.nlm.nih.gov/sra/PRJNA1233780. The other data generated in the present study may be requested from the corresponding author.

Authors' contributions

FFL, QQ, SL and HGW contributed to the research conception and design. FFL, YQ and YH performed the experiments and drafted the manuscript. YL, KG, HRL and CFG analyzed and interpreted the raw data. FFL, QQ, YL, KG, HRL and CFG confirm the authenticity of all the raw data. All authors read and approved the final version of the manuscript.

Ethics approval and consent to participate

The present study was approved by the Animal Welfare Committee of Longhua Hospital, Shanghai University of TCM (approval no. LHERAW-24010; Shanghai, China).

Patient consent for publication

Not applicable.

Competing interests

The authors declare that they have no competing interests.

References

1. Joaquin Garcia A, Rediti M, Venet D, Majjaj S, Kammler R, Munzone E, Gianni L, Thürlimann B, Laáng I, Colleoni M, *et al*: Differential benefit of metronomic chemotherapy among triple-negative breast cancer subtypes treated in the IBCSG trial 22-00. Clin Cancer Res 29: 4908-4919, 2023.
2. Siegel RL, Giaquinto AN and Jemal A: Cancer statistics, 2024. CA Cancer J Clin 74: 12-49, 2024.
3. Rusakiewicz S, Tyekucheva S, Tissot-Renaud S, Chaba K, Imbimbo M, Benedetti F, Kammler R, Hornfeld J, Munzone E, Gianni L, *et al*: Multiplexed high-throughput immune cell imaging in patients with high-risk triple negative early breast cancer: Analysis from the international breast cancer study group (IBCSG) trial 22-00. Eur J Cancer 200: 113535, 2024.
4. Hanna D, Merrick S, Ghose A, Devlin MJ, Yang DD, Phillips E, Okines A, Chopra N, Papadimatraki E, Ross K, *et al*: Real world study of sacituzumab govitecan in metastatic triple-negative breast cancer in the United Kingdom. Br J Cancer 130: 1916-1920, 2024.
5. Dent R, André F, Gonçalves A, Martin M, Schmid P, Schütz F, Kümmel S, Swain SM, Bilici A, Loirat D, *et al*: IMpassion132 double-blind randomised phase III trial of chemotherapy with or without atezolizumab for early relapsing unresectable locally advanced or metastatic triple-negative breast cancer. Ann Oncol 35: 630-642, 2024.
6. Lynce F, Mainor C, Donahue RN, Geng X, Jones G, Schlam I, Wang H, Toney NJ, Jochems C, Schlom J, *et al*: Adjuvant nivolumab, capecitabine or the combination in patients with residual triple-negative breast cancer: The OXEL randomized phase II study. medRxiv [Preprint]: 2023.12.04.23297559, 2023.
7. Schmid P, Cortes J, Pusztai L, McArthur H, Kümmel S, Bergh J, Denkert C, Park YH, Hui R, Harbeck N, *et al*: Pembrolizumab for early triple-negative breast cancer. N Engl J Med 382: 810-821, 2020.
8. Wang S, Li J, Xu S, Wang N, Pan B, Yang B, Zheng Y, Zhang J, Peng F, Peng C and Wang Z: Baohuoside I chemosensitises breast cancer to paclitaxel by suppressing extracellular vesicle/CXCL1 signal released from apoptotic cells. J Extracell Vesicles 13: e12493, 2024.
9. Wu C, Sun C, Liu G, Qin Y, Xue X, Wu X, Wang Q, Liu J, Ye Z, Li Q, *et al*: Effectiveness of the sanyin formula plus chemotherapy on survival in women with triple-negative breast cancer: A randomized controlled trial. Front Oncol 12: 850155, 2022.
10. Kan LLY, Chan BCL, Leung PC and Wong CK: Natural-product-derived adjunctive treatments to conventional therapy and their immunoregulatory activities in triple-negative breast cancer. Molecules 28: 5804, 2023.
11. Alam S, Lee J and Sahebkar A: Curcumin in cancer prevention: Insights from clinical trials and strategies to enhance bioavailability. Curr Pharm Des 30: 1838-1851, 2024.
12. Zhao P, Qiu J, Pan C, Tang Y, Chen M, Song H, Yang J and Hao X: Potential roles and molecular mechanisms of bioactive ingredients in Curcumae Rhizoma against breast cancer. Phytomedicine 114: 154810, 2023.
13. Zhang R, Pan T, Xiang Y, Zhang M, Xie H, Liang Z, Chen B, Xu C, Wang J, Huang X, *et al*: Curcumenol triggered ferroptosis in lung cancer cells via lncRNA H19/miR-19b-3p/FTH1 axis. Bioact Mater 13: 23-36, 2021.
14. Mao Z, Zhong L, Zhuang X, Liu H and Peng Y: Curcumenol targeting YWHAG inhibits the pentose phosphate pathway and enhances antitumor effects of cisplatin. Evid Based Complement Alternat Med 2022: 3988916, 2022.
15. Fuhrmann J, Rurainski A, Lenhof HP and Neumann D: A new Lamarckian genetic algorithm for flexible ligand-receptor docking. J Comput Chem 31: 1911-1918, 2010.
16. Livak KJ and Schmittgen TD: Analysis of relative gene expression data using real-time quantitative PCR and the 2(-Delta Delta C(T)) method. Methods 25: 402-408, 2001.
17. Liu Q, Li R and Lin J: No difference among inhaled anesthetics on the growth and metastasis of murine 4T1 breast cancers in a mouse model of spontaneous metastasis. Front Pharmacol 13: 794109, 2022.
18. Fang Y, Wang Y, Ma H, Guo Y, Xu R, Chen X, Chen X, Lv Y, Li P and Gao Y: TFAP2A downregulation mediates tumor-suppressive effect of miR-8072 in triple-negative breast cancer via inhibiting SNAI1 transcription. Breast Cancer Res 26: 103, 2024.
19. Nielsen AJ, Albert GK, Sanchez A, Chen J, Liu J, Davalos AS, Geng D, Bradeen X, Hintzsche JD, Robinson W, *et al*: DNA-PK inhibition enhances neoantigen diversity and increases T cell responses to immunoresistant tumors. J Clin Invest 134: e180278, 2024.
20. Basu A, Ramamoorthi G, Albert G, Gallen C, Beyer A, Snyder C, Koski G, Disis ML, Czerniecki BJ and Kodumudi K: Differentiation and regulation of TH cells: A balancing Act for cancer immunotherapy. Front Immunol 12: 669474, 2021.
21. Boieri M, Malishkevich A, Guennoun R, Marchese E, Kroon S, Trerice KE, Awad M, Park JH, Iyer S, Kreuzer J, *et al*: $CD4^+$ T helper 2 cells suppress breast cancer by inducing terminal differentiation. J Exp Med 219: e20201963, 2022.
22. Feng S, Li S, Wu Z, Li Y, Wu T, Zhou Z, Liu X, Chen J, Fu S, Wang Z, *et al*: Saffron improves the efficacy of immunotherapy for colorectal cancer through the IL-17 signaling pathway. J Ethnopharmacol 337: 118854, 2025.
23. Chen X, Cui H, Qin L, Liu R, Fang F and Wang Z: Soybean lecithin-gallic acid complex sensitizes lung cancer cells to radiation through ferroptosis regulated by Nrf2/SLC7A11/GPX4 pathway. Nutrients 17: 1262, 2025.
24. Wang Y, Guan WX, Zhou Y, Zhang XY and Zhao HJ: Red ginseng polysaccharide promotes ferroptosis in gastric cancer cells by inhibiting PI3K/Akt pathway through down-regulation of AQP3. Cancer Biol Ther 25: 2284849, 2024.
25. Ning Y, Fang S, Zhang R, Fang J, Lin K, Ding Y, Nie H, Zhou J, Zhao Q, Ke H, *et al*: Simvastatin induces ferroptosis and activates anti-tumor immunity to sensitize anti-PD-1 immunotherapy in microsatellite stable gastric cancer. Int Immunopharmacol 142: 113244, 2024.
26. Paulino P, Vitari G, Rezende A, Couto J, Antunes S, Domingos A, Peckle M, Massard C, Araújo F and Santos H: Characterization of the rhipicephalus (Boophilus) microplus sialotranscriptome profile in response to Theileria equi infection. Pathogens 10: 167, 2021.
27. Shih VFS, Kearns JD, Basak S, Savinova OV, Ghosh G and Hoffmann A: Kinetic control of negative feedback regulators of NF-kappaB/RelA determines their pathogen- and cytokine-receptor signaling specificity. Proc Natl Acad Sci USA 106: 9619-9624, 2009.
28. Wang X, Xue X, Pang M, Yu L, Qian J, Li X, Tian M, Lyu A, Lu C and Liu Y: Epithelial-mesenchymal plasticity in cancer: Signaling pathways and therapeutic targets. MedComm (2020) 5: e659, 2024.
29. Zhang Y, Yang Y, Qi X, Cui P, Kang Y, Liu H, Wei Z and Wang H: SLC14A1 and TGF-β signaling: A feedback loop driving EMT and colorectal cancer metachronous liver metastasis. J Exp Clin Cancer Res 43: 208, 2024.

30. Li Y, Lin H, Sun Y, Zhao R, Liu Y, Han J, Zhu Y, Jin N, Li X, Zhu G and Li Y: Platycodin D2 mediates incomplete autophagy and ferroptosis in breast cancer cells by regulating mitochondrial ROS. Phytother Res 39: 581-592, 2025.
31. Xu G, Zhou Q, Qi J, Li Z, Yin L, Li Z, Lu C, Zhao B and Shen Y: Resveratrol-derived inhibitors of the E3 ubiquitin ligase PELI1 inhibit the metastasis of triple-negative breast cancer. Eur J Med Chem 265: 116060, 2024.
32. Xie J, Deng X, Xie Y, Zhu H, Liu P, Deng W, Ning L, Tang Y, Sun Y, Tang H, *et al*: Multi-omics analysis of disulfidptosis regulators and therapeutic potential reveals glycogen synthase 1 as a disulfidptosis triggering target for triple-negative breast cancer. MedComm (2020) 5: e502, 2024.
33. Zou Y, Yang A, Chen B, Deng X, Xie J, Dai D, Zhang J, Tang H, Wu T, Zhou Z, *et al*: crVDAC3 alleviates ferroptosis by impeding HSPB1 ubiquitination and confers trastuzumab deruxtecan resistance in HER2-low breast cancer. Drug Resist Updat 77: 101126, 2024.
34. Su Z, Liu Y, Wang L and Gu W: Regulation of SLC7A11 as an unconventional checkpoint in tumorigenesis through ferroptosis. Genes Dis 12: 101254, 2024.
35. Zhou D, Sun L, Li J and Yang Y: Schisandrin B inhibits inflammation and ferroptosis in S.aureus-induced mastitis through regulating SIRT1/p53/SLC7A11 signaling pathway. Int Immunopharmacol 137: 112430, 2024.
36. Qiu Y, Wang H, Guo Q, Liu Y, He Y, Zhang G, Yang C, Du Y and Gao F: CD44s-activated tPA/LRP1-NFκB pathway drives lamellipodia outgrowth in luminal-type breast cancer cells. Front Cell Dev Biol 11: 1224827, 2023.
37. Wu Y, Dai S, Zhang Y, Li Z, Zhu B, Liu Q, Wo L, Yu Z, Yuan X and Dou X: Atractylenolide II combined with Interferon-γ synergistically ameliorates colorectal cancer progression in vivo and in vitro by blocking the NF-kB p65/PD-L1 pathway. J Cancer 15: 4328-4344, 2024.
38. Ayaz MO, Bhat AQ, Akhter Z, Badsera N, Hossain MM, Showket F, Parveen S, Dar MS, Tiwari H, Kumari N, *et al*: Identification of a novel GSK3β inhibitor involved in abrogating KRas dependent pancreatic tumors in Wnt/beta-catenin and NF-kB dependent manner. Life Sci 351: 122840, 2024.
39. Pasha A, Kumar K, Heena SK, Arnold Emerson I and Pawar SC: Inhibition of NF-kB and COX-2 by andrographolide regulates the progression of cervical cancer by promoting PTEN expression and suppressing PI3K/AKT signalling pathway. Sci Rep 14: 12020, 2024.
40. Barnes P, Mensah A, Derkyi-Kwarteng L, Adankwa E, Agbo E, Yahaya ES, Amoani B, Adjei G, Ka-Chungu SMA, Akakpo PK, *et al*: Prognostic significance of nuclear factor kappa B (p65) among breast cancer patients in cape coast teaching hospital. Med Princ Pract 33: 1-11, 2024 (Epub ahead of print).
41. Huang F, Dai Z, Yu J, Wang K, Chen C, Chen D, Zhang J, Zhao J, Li M, Zhang W, *et al*: RBM7 deficiency promotes breast cancer metastasis by coordinating MFGE8 splicing switch and NF-kB pathway. Elife 13: RP95318, 2024.
42. He XY, Xiong XJ, Liu MJ, Liang JT, Liu FY, Xiao JY and Wu LJ: Dahuang zhechong pill alleviates liver fibrosis progression by regulating p38 MAPK/NF-κ B/TGF-β1 pathway. Chin J Integr Med 30: 1113-1120, 2024.
43. Mazi FA, Cakiroglu E, Uysal M, Kalyoncu M, Demirci D, Sozeri PYG, Yilmaz GO, Ozhan SE and Senturk S: The paracaspase MALT1 is a downstream target of Smad3 and potentiates the crosstalk between TGF-β and NF-kB signaling pathways in cancer cells. Cell Signal 105: 110611, 2023.
44. Zhao M, Qiu D, Miao X, Yang W, Li S, Cheng X, Tang J, Chen H, Ruan H, Liu Y, *et al*: Melatonin delays arthritis inflammation and reduces cartilage matrix degradation through the SIRT1-mediated NF-κB/Nrf2/TGF-β/BMPs pathway. Int J Mol Sci 25: 6202, 2024.
45. Cai Z, Gao L, Hu K and Wang QM: Parthenolide enhances the metronomic chemotherapy effect of cyclophosphamide in lung cancer by inhibiting the NF-kB signaling pathway. World J Clin Oncol 15: 895-907, 2024.
46. Louault K, Blavier L, Lee MH, Kennedy RJ, Fernandez GE, Pawel BR, Asgharzadeh S and DeClerck YA: Nuclear factor-κB activation by transforming growth factor-β1 drives tumour microenvironment-mediated drug resistance in neuroblastoma. Br J Cancer 131: 90-100, 2024.
47. Li Z, Hao E, Cao R, Lin S, Zou L, Huang T, Du Z, Hou X and Deng J: Analysis on internal mechanism of zedoary turmeric in treatment of liver cancer based on pharmacodynamic substances and pharmacodynamic groups. Chin Herb Med 14: 479-493, 2022.
48. Chen X, Pei L, Zhong Z, Guo J, Zhang Q and Wang Y: Anti-tumor potential of ethanol extract of *Curcuma phaeocaulis* Valeton against breast cancer cells. Phytomedicine 18: 1238-1243, 2011.
49. Hu C, Li M, Guo T, Wang S, Huang W, Yang K, Liao Z, Wang J, Zhang F and Wang H: Anti-metastasis activity of curcumin against breast cancer via the inhibition of stem cell-like properties and EMT. Phytomedicine 58: 152740, 2019.
50. Li M, Guo T, Lin J, Huang X, Ke Q, Wu Y, Fang C and Hu C: Curcumin inhibits the invasion and metastasis of triple negative breast cancer via Hedgehog/Gli1 signaling pathway. J Ethnopharmacol 283: 114689, 2022.
51. Tian NN, Zheng YB, Li ZP, Zhang FW and Zhang JF: Histone methylatic modification mediates the tumor-suppressive activity of curcumol in hepatocellular carcinoma via an Hotair/EZH2 regulatory axis. J Ethnopharmacol 280: 114413, 2021.
52. Al-Amin M, Eltayeb NM, Hossain CF, Rahiman SSF, Khairuddean M and Muhamad Salhimi S: Bioactive compounds from Curcuma aeruginosa and the effect of comosone II on the migration and invasion of breast cancer cells. J Asian Nat Prod Res 4: 1-12, 2022 (Epub ahead of print).
53. Shen Z, Yu N, Zhang Y, Jia M, Sun Y, Li Y and Zhao L: The potential roles of HIF-1α in epithelial-mesenchymal transition and ferroptosis in tumor cells. Cell Signal 122: 111345, 2024.
54. Fan J, Lin H, Luo J and Chen L: 4-Methoxydalbergione inhibits the tumorigenesis and metastasis of lung cancer through promoting ferroptosis via the DNMT1/system Xc-/GPX4 pathway. Mol Med Rep 31: 19, 2025.
55. Rossi T, Iorio E, Chirico M, Pisanu ME, Amodio N, Cantafio MEG, Perrotta I, Colciaghi F, Fiorillo M, Gianferrari A, *et al*: BET inhibitors (BETi) influence oxidative phosphorylation metabolism by affecting mitochondrial dynamics leading to alterations in apoptotic pathways in triple-negative breast cancer (TNBC) cells. Cell Prolif 57: e13730, 2024.
56. Yang X, Yang R, Zhang Y, Shi Y, Ma M, Li F, Xie Y, Han X and Liu S: Xianlinglianxiafang inhibited the growth and metastasis of triple-negative breast cancer via activating PPARγ/AMPK signaling pathway. Biomed Pharmacother 165: 115164, 2023.
57. Chen G, Wang Y, Li M, Xu T, Wang X, Hong B and Niu Y: Curcumol induces HSC-T6 cell death through suppression of Bcl-2: Involvement of PI3K and NF-κB pathways. Eur J Pharm Sci 65: 21-28, 2014.
58. Al-Amin M, Eltayeb NM, Khairuddean M and Salhimi SM: Bioactive chemical constituents from Curcuma caesia Roxb. rhizomes and inhibitory effect of curcuzederone on the migration of triple-negative breast cancer cell line MDA-MB-231. Nat Prod Res 35: 3166-3170, 2021.
59. Zhou Y, Moon JH, Kim JT, Qiu S, Lee SB, Park HJ, Son MJ, Lee GY, Kwon JW, Park SH, *et al*: Curcumol metabolized by rat liver S9 fraction and orally administered in mouse suppressed the proliferation of colon cancer in vitro and in vivo. Food Sci Biotechnol 33: 171-180, 2023.
60. Sheng W, Ding J, Liu L, Wang N, Lu B, You X, He Q and Zhou Q: Curcumol inhibits the development of prostate cancer by miR-125a/STAT3 axis. Evid Based Complement Alternat Med 2022: 9317402, 2022.
61. Yu C, Xing H, Fu X, Zhang Y, Yan X, Feng J, He Z, Ru L, Huang C and Liang J: Effect and mechanisms of shikonin on breast cancer cells in vitro and in vivo. BMC Complement Med Ther 24: 389, 2024.
62. Simões RV, Serganova IS, Kruchevsky N, Leftin A, Shestov AA, Thaler HT, Sukenick G, Locasale JW, Blasberg RG, Koutcher JA and Ackerstaff E: Metabolic plasticity of metastatic breast cancer cells: Adaptation to changes in the microenvironment. Neoplasia 17: 671-684, 2025.
63. He D, Tan XN, Li LP, Gao WH, Tian XF and Zeng PH: Brazilin actuates ferroptosis in breast cancer cells via p53/SLC7A11/GPX4 signaling pathway. Chin J Integr Med 30: 1001-1006, 2024.
64. Yang R, Xie Y, Li Q, Ye Y, Shi Y, Zhao X, Wu C, Xu Y, Wang R, Zhang Y, *et al*: Ruyiping extract reduces lung metastasis in triple negative breast cancer by regulating macrophage polarization. Biomed Pharmacother 141: 111883, 2021.
65. Uribesalgo I, Hoffmann D, Zhang Y, Kavirayani A, Lazovic J, Berta J, Novatchkova M, Pai TP, Wimmer RA, László V, *et al*: Apelin inhibition prevents resistance and metastasis associated with anti-angiogenic therapy. EMBO Mol Med 11: e9266, 2019.
66. Masoumi J, Zainodini N, Basirjafar P, Tavakoli T, Zandvakili R, Nemati M, Ramezani M, Rezayati MT, Ayoobi F, Khademalhosseini M, *et al*: Apelin receptor antagonist boosts dendritic cell vaccine efficacy in controlling angiogenic, metastatic and apoptotic-related factors in 4T1 breast tumor-bearing mice. Med Oncol 40: 179, 2023.

67. Deng R, Zong GF, Wang X, Yue BJ, Cheng P, Tao RZ, Li X, Wei ZH and Lu Y: Promises of natural products as clinical applications for cancer. Biochim Biophys Acta Rev Cancer 1880: 189241, 2025.
68. Li J, Sun Y, Li G, Cheng C, Sui X and Wu Q: The extraction, determination, and bioactivity of curcumenol: A comprehensive review. Molecules 29: 656, 2024.
69. Zhang LS, Shen SN, Gao YL, Shi SY, Zhou CX, Mo JX, Xu YK, Lin LG and Gan LS: Tautomerism and bioactivities of curcumenol, a common sesquiterpenoid widely existing in edible plants. Food Funct 10: 1288-1294, 2019.